BUDAPEST UNIVERSITY OF TECHNOLOGY AND ECONOMICS
FACULTY OF CHEMICAL TECHNOLOGY AND BIOTECHNOLOGY

Optimization of membrane electrode assembly for PEM fuel cells

Danielle Verde Nolasco
Supervisor: Dr. András Tompos
Internal consultant: Dr. Imre Miklós Szilágyi
External consultant: Dr. Gábor Pál Szijjártó

RENEWABLE ENERGY RESEARCH GROUP
INSTITUTE OF MATERIAL AND ENVIRONMENTAL CHEMISTRY
RESEARCH CENTRE FOR NATURAL SCIENCES

Budapest

2021

Index

1. Introduction 5
2. State of the art 7
2.1. Working principle 7
2.2. Fuel Cell types 13
2.2.1. Proton Exchange Membrane Fuel Cell (PEMFC) 13
2.2.2. Direct Methanol Fuel Cell (DMFC) 14
2.2.3. Alkaline Fuel Cells (AFC) 15
2.2.4. Phosphoric Acid Fuel Cells (PAFC) 16
2.2.5. Molten Carbonate Fuel Cells (MCFC) 16
2.2.6. Solid Oxide Fuel Cells (SOFC) 17
2.3. Engineering approaches and challenges in PEMFC development 17
2.4. CO tolerance of PEM fuel cells 23
2.5. Electrochemical Impedance Spectroscopy (EIS) in PEMFC analysis 24
3. Aim of the study 30
4. Experimental 32
4.1. Preparative methods 32
4.1.1. Preparation of catalyst support 32
4.1.2. Addition of Pt to catalyst support 33
4.1.3. Membrane electrode assembly preparation protocol 34
4.2. The fuel cell workstation 35
4.3. Measuring methods 35
4.3.1. MEA characterization before FC testing 35
4.3.2. NEDC protocol 37
4.3.2.1. Activation of the MEA 37
4.3.2.2. Polarization curve 38
4.3.2.3. Validation of FC-DLC test and regeneration 40
4.3.2.4. Determination of rate of degradation 41
4.3.3. Determination of Power maximum 44
4.3.4. Cyclic voltammetry (CV) measurements 44
4.3.4.1. CV measurements on rotating disc electrode (RDE) 45
4.3.5. CV measurements on Fuel Cell (FC) 46
4.3.6. Potentiostatic Electrochemical Impedance Spectroscopy (PEIS) measurements on Fuel Cell 47
4.3.7. The applied different membrane electrode assembly compositions 48
4.3.8. Scaling up from 16 cm^2 MEA to 50 cm^2 MEA 49

5. Results and Discussion 50
5.1. MEA characterization before FC testing 50
5.2. Optimization of Pt loading of the MEAs 51
5.3. Fuel Cell testing of anode catalysts 55
5.4. Hydrogen oxidation reaction of anode catalysts on RDE 57
5.5. Potentiostatic Electrochemical Impedance Spectroscopy 58
5.6. Scaling up from 16 cm^2 to 50 cm^2 64
6. Summary 69
7. Összefoglalás 71
8. Acknowledgment 73
References 74
Appendix 78

Abbreviations

AFC	Alkaline Fuel Cells
CNC	Computerized numerical control
CV	Cyclic voltammetry
DLC	Dynamic load-cycle
DMFC	Direct Methanol Fuel Cell
ECSA	Electrochemical active surface area
EDS	Energy-dispersive X-ray spectroscopy
EG	Ethylene-glycol
EIS	Electrochemical Impedance Spectroscopy
FC	Fuel cell
FCEV	Fuel cell electric vehicle
FRA	Frequency response analyzer
GDE	Gas difusion electrode
GDL	Gas diffusion layer
GEIS	Galvanostatic electrochemical impedance spectroscopy
HOR	Hydrogen oxidation reaction
MCFC	Molten Carbonate Fuel Cells
MEA	Membrane Electrode Assembly
NEDC	New European Driving Cycle
ORR	Oxygen reduction reaction
PAFC	Phosphoric Acid Fuel Cells
PEIS	Potentiostatic electrochemical impedance spectroscopy
PEM	Proton Exchange Membrane
PEMFC	Proton Exchange Membrane Fuel Cell
PFSA	Perfluoro sulfonic acid
PTFE	Polytetrafluorethylene
PV	Photovoltaic
RDE	Rotating Disc Electrode
SEM	Scanning electron microscopy
SOFC	Solid Oxide Fuel Cells
XRD	X-Ray diffraction

1. Introduction

The increase of the population and the increase of energy demand have attracted research interest to find alternative energy production routes. The increase of demand for energy, the current scenario of limited fuel energy sources, and the drawbacks of this energy to the environment make clean energies, as fuel cells, be a potential substitute for fuel energy in the future. Fuel cells are devices which converts chemical reactions into energy, and it consists of two electrodes: an anode and a cathode [1]. Proton Exchange Membrane Fuel Cell (PEMFC) is the most used type of fuel cell. Nowadays, humanity is facing with global climate change, increasing pollution levels, and the possibility that fossil resources could be depleted. Therefore, fuel cells using green or decarbonized hydrogen have become an environmentally benign technology that does not have any hazardous impact. PEM fuel cell operates at high electric efficiency, above 50 %, reaching 80 % if heat is recovered [3] [4]. It operates with hydrogen and oxygen and only generates heat and water by-products.

Batteries and fuel cells are similar in sense that both are electrochemical energy converters. However, the main difference between them is that the battery contains all chemical species participating in the charge-discharge cycle, and the extent of storage is determined by the amount of chemical substances stored [1]. However, a fuel cell can produce electricity as long as the fuel and oxidant are supplied in the electrodes [1]. The electrodes essentially consist of electrocatalysts, on which the electrochemical reactions are completed. In PEMFC generally platinum is used as electrocatalyst. Nevertheless, Pt is an expensive material that increases the final price of the PEMFC production, limiting the usage on a large scale. This is why it is important to study and develop new techniques to decrease the cell's Pt content. The study of the minimum Pt content used in the cell and keeping the performance is essential for developing this type of device. The first early fuel cell used catalysts with a platinum content of up to 4 mg/cm^2 specific Pt content related to geometrical surface of the membrane electrode assembly [5]. Recently, the common platinum loading is 0.2-0.8 mg/cm^2 [5], which still has to be decreased for making large-scale commercial applications viable.

The performance of the PEMFC is dependent on the working parameters applied to the fuel cell. These parameters are the pressure of reactants, temperature, and flow. Changing these parameters can positively or negatively affect the overall performance of the PEM fuel cell, being necessary to define the perfect working conditions. Degradation and stability of the stack components such as membranes, catalysts and gas diffusion layers, are some of the challenges

for PEM fuel cells that are responsible for delaying commercialization of the PEMFC technology as these components are susceptible to physical and chemical degradation as well as electro corrosion [6].

The suitable working conditions and membrane electrode assembly composition have to be determined at laboratory scale. However, it is essential to scale up the device to verify if the PEMFC keeps the same results and efficiency in a bigger cell. The size of the cell can affect the resistance, which can affect the cell's efficiency. The Renewable Energy Research Group staff at the Institute of Materials and Environmental Chemistry of the Research Centre of Natural Sciences is working to address these challenges, to which I have joined in my master work.

2. State of the art

2.1. Working principle

Fuel cells are devices, electrochemical cells which generate electrical energy through reduction and oxidation reactions separated from each other in space. The fuel cells consist of two electrodes: an anode (where the oxidation of hydrogen/methanol occurs) and a cathode (where the reduction of oxygen takes place). The by-products generated in these processes' reaction heat, carbon dioxide (in direct methanol fuel cells), and water [1].

Electrocatalysts designed for PEMFC was studied for the present MSc thesis. ***Figure 1*** shows the components and configuration of the PEM Fuel Cell. The main components are the porous gas diffusion electrode, the proton-conducting electrolyte, anodic and cathodic catalyst layers, current collectors, and cell stacks connecting in series or parallel [1].

At the anode, the negative electrode of the fuel cell, the electrons produced in hydrogen oxidation reaction (HOR) conducted through the electric circuit. At the cathode, the positive electrode of the fuel cell, the electrons back from the external circuit reduces oxygen over the catalysts that form water with hydrogen ions passing through the electrolyte. All the reaction occurs in the cell stack that is built in a module including fuel, water, and air management. PEMFC single cell is shown schematically in ***Figure 1***.

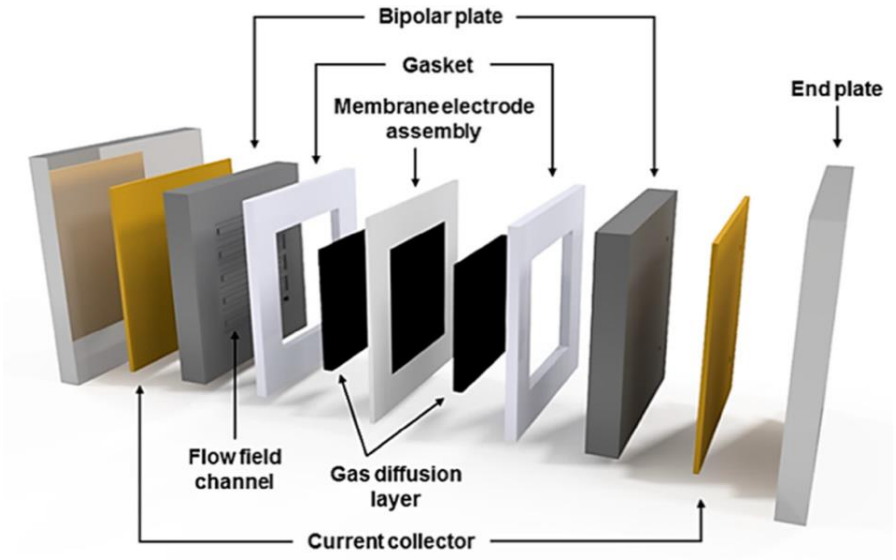

Figure 1. Main components of PEM fuel cell.

PEMFC uses pure hydrogen as fuel. It is the most frequently used type of fuel cells with broad application areas in aerospace, aircraft, road transportation sector, and energy storage [2]. PEMFC was the first type of fuel cells, which has been applied by NASA [1]. Due to low-temperature operation conditions, low weight, it generates a reasonable specific power (W/kg), and power density (W/cm^3), which attracts a lot of interest to use it in transport applications [1] [7].

The membrane electrode assembly is a crucial part of PEMFC. It consists of the catalyst, membrane, and gas diffusion layers. For this MSc project, the Nafion was used as a membrane, separating the reduction and oxidation half-reactions from each other in space as it makes the protons pass through to complete the overall reaction. A membrane has plenty of advantages compared to using liquid for cell constructions, for example, low weight and easy fabrication.

The composition and construction of a membrane electrode assembly have to minimize all forms of over-potential, maximize power density, minimize noble metal loading, functional and thermal and water management, increase or keep the lifetime of PEMFC as required for the power generation, transportation, and portable power application [1]. The ***Figure 2*** shows the working principle of PEMFC.

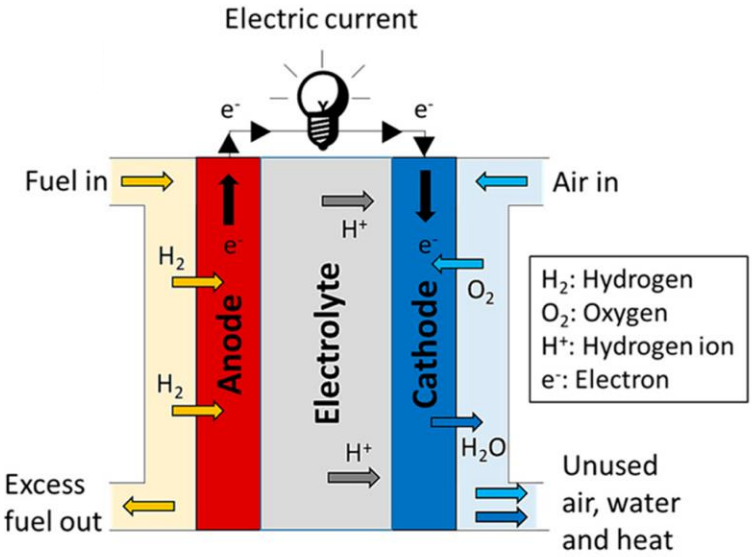

Figure 2. Working theory of the proton-exchange membrane fuel cell

PEM conducts protons from the anode to the cathode of the fuel cell, prevents electronic charge from passing through the membrane and separates the reactant gases [9]. High proton conductivity, low electronic conductivity, low permeability to fuel, good chemical stability, good mechanical properties, and low cost have to be achieved [10]. The most common type of

PEM is the one that utilizes perfluoro sulfonic acid (PFSA) [9]. One example of this type is the Nafion produced from DuPont and applied in the current study. The structure of Nafion is shown in ***Figure 3*** below.

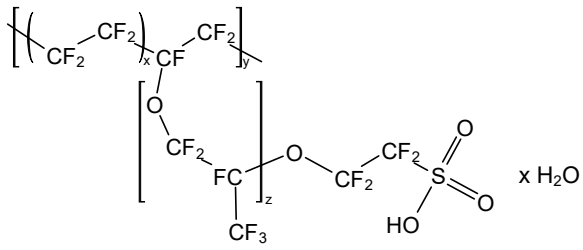

Figure 3. Chemical structure of Nafion

The Nafion membrane has perfluorinated vinyl ether side chains with sulfonate end groups on polytetrafluorethylene (PTFE) backbone [10]. The Teflon backbone provides the hydrophobic behaviour of the membrane. Simultaneously, hydrophilic behaviour attributed to the sulfonic acid groups allows absorption of water by the polymer leading to high hydration of the polymer [10] [11]. In general, in order to increase efficiency of ion conduction of the membrane, the polymer's hydration level should be increased [12]. In the early development of MEA, polytetrafluoroethylene (PTFE, Teflon) was used instead of Nafion, and the catalyst loading was around 10 mg cm^{-2} while it is below 1 mg cm^{-2} when Nafion is used [13].

Other materials have been developing to use instead of Nafion. A nanocomposite membrane has been proposed to overcome the hydration problem of the Nafion membrane [12]. On the other hand, hydrocarbon polymers (sulfonated hydrocarbons) are suggested as substitute Nafion membranes [12]. ***Figure 4*** shows the representation of the Polibenzimidazol chemical structure.

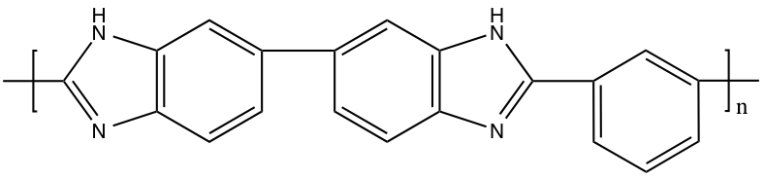

Figure 4. Polibenzimidazol chemical structure

For the PEM fuel cell application, nanostructured carbon materials have been used as support of the active phase of the electrocatalysts due to their high surface area and high electrical conductivity, even though this type of material is more susceptible to corrosion [14] [15]. That is the reason why interest is growing in studies to improve the durability of support

while keeping the catalyst activity [16]. In an electrocatalyst beside the support suitable active phases, such as for example Pt, for hydrogen oxidation and oxygen reduction reaction are required [1]. However, as Pt is a precious metal, it can increase the PEM fuel cell price [5]. This precious metal is deposited over carbon support to create electrocatalyst.

The first early Fuel Cell used catalysts with a platinum content of up to 4 mg/cm^2 [5]. Recently, the common platinum loading is 0.2-0.8 mg/cm^2 [5]. Even this shallow concentration of Pt can significantly increase production's final price for large-scale commercial applications. In my work platinum content was analyzed between 0.05 – 0.2 mg/cm^2.

In formation of membrane electrode assemblies first a suspension of the catalysts, so called catalyst ink, is prepared. Then various techniques are used to distribute evenly the ink over the surface of gas diffusion layer (GDL) or the membrane including spreading, painting and screen printing [17]. Accordingly, the catalyst layer (CL) may be loaded over the membrane (Catalyst Coated Membrane – CCM) or the GDL (Catalyst Coated GDL – CCG) [17]. In the spreading technique, the catalyst is spread on the surface using a heavy stainless-steel cylinder on a flat surface or rolling in between two rotating cylinders [17]. In the ink painting, catalyst ink is spray-brushed directly onto the GDL [17]. This technique is used in the current project. The other technique used is ink screen printing, which is not widely used for MEA [17]. A screen sieve is held above the substrate in this method while the pre-prepared catalyst slurry or ink is applied over it [17].

The purpose of the gas diffusion layer (GDL) is the effective diffusion of reactant gaes through the catalyst layer, and as well it helps water management of the membrane [5]. The GDL is available in different forms like carbon paper or woven carbon fabrics [18]. The carbon papers are too rigid or too fragile for roll packing. That is the reason why it is less used for mass production [18]. The carbon fabrics are more flexible and can tolerate higher compression loads [18]. From the diverse variety of GDLs available, the Toray paper is the most used because of its low cost [18]. GDLs can be used in PEMFC operating with hydrogen or methanol and can be used for acid fuel cells (PAFC) [18]. For my MSc thesis, porous carbon paper was used in a dimension of 16 cm^2.

The bipolar plate is an essential and fundamental fuel cell building element [19]. They provide even distribution of reactant gases, conduct electrical current from cell to cell, helps heat management of the cell. It is a significant factor in determining the fuel cell's gravimetric and volumetric power density. It contributes to more than 80% of the total weight stack and almost all volume [19]. That is the main reason of development of bipolar plates has been

attracting interest, as the improvement on this part of the fuel cell can consequently improve the fuel cell performance weight and cost of the stacks [19].

The main goal of the bipolar plates is to carry fuel and air to the respective electrode and disperse the reactants in a controlled way while removing the excess water [19]. As it is an essential part of the fuel cell stack and contributes to more than half of their size and weight, improvements in the working and design of the bipolar plates can reduce the fuel cell's overall cost. Researches show that the bipolar plates contribute from 12% to 68% of the total stack cost [19].

The main features desired in a bipolar plate are: high electrical conductivity, low contact resistance with the GDL, good thermal conductivity, thermal stability, gas impermeability, high mechanical strength, corrosion resistance, resistance to ion-leaching, thin and lightweight properties, low cost, and ease of manufacturing and environmentally benign. The most common types of material used for bipolar plate production and their respective advantages and disadvantages are listed in ***Table 1*** below.

Table 1. Advantages, disadvantages and processing options for Bipolar Plates made by graphite, metallic, and coated metallic materials

	Graphite	**Metallic**	**Coated metallic**
Advantages	High electrical conductivity Corrosion-resistant Low contact resistance with GDL Good prototyping material High-temperature operation for pyrolytic impregnation	High electrical conductivity High thermal conductivity High strength High-temperature operation Gas-impermeable Thin plates Amenable to a range of processing and forming techniques Easily recyclable	As for metallic
Disadvantages	Flow-field marching required (expensive) Material is expensive Permeable to hydrogen (requires impregnation Brittle Must be made thick	Prone to corrosion Form insulating oxides (increased contact resistance) Ion leaching (cations degrade membrane performance) Corrosion-resistant metals and alloys are expensive Corrosion-resistant coating may be necessary	Extra processing and expensive

Processing options	Computerized numerical control (CNC) milling	CNC milling Stamping/embossing Foaming Die forging Etching Note: the range of forming methods applicable depends on the metal and size of plate	Depends on nature of coating and order in which coating is applied

Proton Exchange Membrane Fuel Cells (PEMFC) has some advantages like low operating temperature, high current density, low weight, and compactness, making them make a wide variety of power applications [33]. The main application area of PEM is transportation (Fuel Cell Electric Vehicles – FCEV), stationary and portable applications [33]. The summary of the main applications for PEMFC is shown in ***Table 2*** below.

Table 2. Applications of PEMFC

Application	Function	Power	Fuel	Comments
Submarine Type 212	Power supply	300kW	Hydrogen stored in the metal hydrides	Propulsion: combination of marine diesel engine, FC and electric motor
Train	Power supply	200kW	High-pressure gaseous hydrogen in the cylinder	Siemens-Ballard Mireo Plus H 160km/h speed
Car Toyota Mirai	Power supply	114kW	High-pressure gaseous hydrogen in the cylinder	One of the first mass produced and commercially sold FCEV
Hybrid power bus	Power supply	50kW	Compressed hydrogen in the cylinder	Efficiency: 40%, Mean power consumption: 17-24kW
Powered bicycle	Power supply	300W	Hydrogen stored in the metal hydrides	Efficiency: 35%. Distance-to-fuel ratio: 1,35km/g
Lightweight powered vehicle	Power Supply	5kW	High-pressure gaseous hydrogen in the cylinder	Drive over a 100km run at a speed of 18 km/h
Sailing yacht	APU (auxiliary	300W	Hydrogen produced by LPG via a series	Used as auxiliary power using bottled LPG as fuels

	power units)		of processor on-board system	
Stationary power generator	Power supply	5kW	Commercially available 15 MPa hydrogen cylinder	Efficiency: more than 30% in fully loaded operation. Operated three h at 5kW with two 50 liter hydrogen cylinders
Uninterrupted power supply	Power supply	2kW	Hydrogen produced by methanol via fuel processing	Total cost was strongly dependent on the service time
Portable computer	Power supply	46W	Hydrogen stored in the metal hydrides	Trouble-free startup of the portable computer

2.2. Fuel Cell types

Fuel cells can be classified according to the applied electrolytes. The most important types are the followings:

1. Proton Exchange Membrane (polymer electrolyte) Fuel cells (PEMFC)
2. Direct Methanol Fuel Cell (DMFC)
3. Alkaline Fuel Cells (AFC)
4. Phosphoric Acid Fuel Cells (PAFC)
5. Molten Carbonate Fuel Cells (MCFC)
6. Solid Oxide Fuel Cells (SOFC)

Fuel cell types are summarized in ***Figure 5***.

2.2.1. Proton Exchange Membrane Fuel Cell (PEMFC)

The PEMFC, beside the advantage of high-power density and green operation [16], has some disadvantages, too, compared to other types of energy production. Its production is expensive because of Pt in the electrodes and its operation has a high-cost due to need of the high purity hydrogen [20]. High temperature PEMFCs are under development in order to increase fuel tolerance of the technology. Additionally, CO tolerant electrocatalysts has to be developed if hydrogen is derived even from fossil or biological resources and CO impurities pose a challenge to the operation of PEMFC [1].

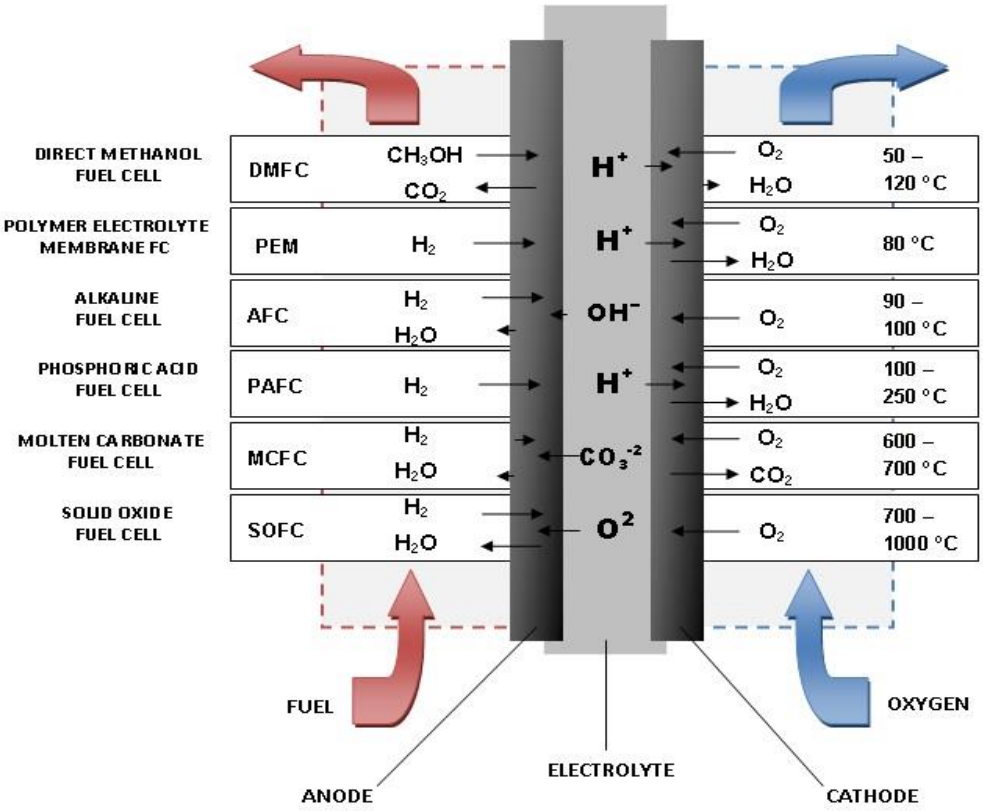

Figure 5. Electrode processes taking place in different fuel cells

2.2.2. Direct Methanol Fuel Cell (DMFC)

Direct Methanol Fuel Cell (DMFC) uses liquid methanol as the fuel. In DMFC, the electrolyte is also a proton exchange membrane (PEM), as in the case of PEMFC. Advantages of this fuel cell type are mild operation conditions, and easy methanol fuel storage, which makes DMFC applicable for portable operations [1] [21] [22]. Methanol is cheap, easy to store and handled, and readily available, consequently being an attractive type of fuel to be used [1].

DMFC is divided into two types: active and passive. The active types use pumps and blowers to feed with reagents and take of the products, while the passive use diffusion and natural convection for take-off the products [23]. The working processes in DMFC consist of the oxidation of methanol and oxygen reduction [24]. The oxidation reaction is given by:

$$Anode\ CH_3OH + H_2O \rightarrow CO_2 + 6H^+ + 6e^- \qquad \textbf{\textit{Eq. 1}}$$

For the cathode side, oxygen from the air is reduced and reacts with the proton to form water. The reduction reaction is given by:

$$Cathode \quad {}^{3}/_{2}\, O_2 + 6H^+ + 6e^- \rightarrow 3H_2O \qquad \textbf{\textit{Eq. 2}}$$

The overall reaction in the cell is given by:

$$CH_3OH + {}^{3}/_{2}\, O_2 \rightarrow 3H_20 + CO_2 \qquad \textbf{\textit{Eq. 3}}$$

Some of the drawbacks regarding DMFC are sluggish electrode reactions and methanol crossover (MCO), which is defined as methanol transport through the anode to cathode membrane [25] [26], which reduces the performance of the DMFC [5]. The factors those influence the MCO are methanol concentration, membrane thickness, and weight, operation conditions. [27]. Compared to a hydrogen fuel cell, the power density of DMFC is smaller [26]. The Pt loading has to be reduced also significantly, in order to reach a lower commercialization cost of DMFC and be more attractive to the market. [26]

2.2.3. Alkaline Fuel Cells (AFC)

Alkaline fuel cells convert gaseous hydrogen and gaseous oxygen into electricity using potassium hydroxide (30% - 45% KOH) in a temperature range of 293K to 363K [1]. Four types of AFC can be found: (1) cell with a free liquid electrolyte between two porous electrodes. (2) ELOFLUX cell with liquid KOH in the pore-systems. (3) matrix cell where the electrolyte is fixed in the electrode matrix and (4) the falling film cell [28]. AFC works at substantially lower temperatures than other fuel cells and low pressure [1].

The oxidation reaction is given in the anode by the following reaction:

$$Anode \quad H_2 + 2OH^- \rightarrow 2H_2O + 2e^- \qquad \textbf{\textit{Eq. 4}}$$

The reduction reaction is given in the cathode by the following reaction:

$$Cathode \quad \tfrac{1}{2}O_2 + H_2O + 2e^- \rightarrow 2OH^- \qquad \textbf{\textit{Eq. 5}}$$

The overall reaction is given by:

$$H_2 + \frac{1}{2}O_2 \rightarrow 2H_2O + electrical\ energy + heat \qquad \textbf{Eq. 6}$$

Despite the advantages, AFC has some limitations like the electrolyte is a corrosive material, the lack of effective hydroxide ion conductive membrane, costs of the electrode stacks and fuel cell systems, lifetime of the electrodes, and contamination of CO_2 from the air [1]. The cost issues are attributed to usage of noble metals (for example, Pt) as electrode that increase the overall price. Although, the usage of less expensive materials like nickel and silver reduces the cost, however it reduces the lifetime of the fuel cell, too.

2.2.4. Phosphoric Acid Fuel Cells (PAFC)

Phosphoric Acid Fuel Cells (PAFC) uses liquid phosphoric acid as the electrolyte [1] [29]. PAFC consists of two porous gas diffusion electrodes (cathode and anode) in a porous electrolyte matrix [30]. It operates at high temperatures (423-473 K), and it is an expensive type of fuel cell. However, it is suitable for applications that require high quality [1].

Some of the advantages of PAFC are high catalytic efficiency and minor CO poisoning in high-temperature conditions; consequently, for PAFC, it can be applied less Pt in the surface of the catalyst and tolerate higher CO concentrations. On the other hand, PAFC has some disadvantages, like precious metals are required for the electrode and slow start-up due to slightly higher operation temperature [1].

2.2.5. Molten Carbonate Fuel Cells (MCFC)

Molten Carbonate Fuel Cells (MCFC) works in a range temperature of 873 K to 923 K, and as it is a high-temperature fuel cell, it is suitable to operate in a combined heat and power systems [1]. MCFCs electrolytes consist of molten-carbonate salt mixture suspended in a ceramic matrix solid electrolyte [31].

The oxidation reaction is given in the anode by the following reaction:

$$Anode \quad H_2 + CO_3^{2-} \rightarrow H_2O + CO_2 + 2e^- \qquad \textbf{Eq. 7}$$

The reduction reaction is given in the cathode by the following reaction:

$$Cathode \quad \frac{1}{2}O_2 + CO_2 + 2e^- \rightarrow CO_3^{2-} \qquad \textbf{Eq. 8}$$

The overall reaction is given by:

$$H_2 + \frac{1}{2}O_2 + CO_2 \rightarrow H_2O + CO_2 \qquad \textbf{Eq. 9}$$

Some of the advantages regarding the MCFC are that this type of fuel cell is more resistant to impurities and is not poisoned by CO than the other types of fuel cell [31]. Besides that, MCFC is a comparatively cheaper fuel cell because it does not require precious metal to be used as catalysts [31]. One of the disadvantages of MCFC is the high-temperature working conditions, which decreases the fuel cell's cell life. Molten Carbonate Fuel Cell (MCFC) is not suitable for domestic applications because of its complexity. On the other hand, MCFC has been applied in places, schools, or any high commercial application [1]. In Europe, MCFC has been studied for marine applications [1].

2.2.6. Solid Oxide Fuel Cells (SOFC)

Solid Oxide Fuel Cell is defined as a ceramic multilayer system that works at high temperatures using gaseous fuel and oxidant. It has a great potential for power and heat generation. However, the SOFC has some disadvantages, which creates a barrier to the spread of this fuel cell type. Some of the advantages of SOFCs are that they can provide high system efficiency, higher power density, and a more straightforward design [1]. Solid Oxide Fuel Cell (SOFC) is mainly applied in utility applications because of their low noise and readily available fuel usage [32].

2.3. Engineering approaches and challenges in PEMFC development

In Fuel Cell Stacks, the cells are connected in series to achieve an applicable voltage. These stacks are building blocks for large fuel cell systems. The fuel cell stack with a high number of cells requires a manifold with a uniform flow distribution to each cell [4]. The

configuration of the fuel cell stack and the configuration of the gas flow manifolds for a fuel cell stacks are a vital engineering problem which researchers have been attracting attention for the performance of the stacks [4]. A FC stack is visible on **Figure *6***. **Figure *7*** shows the representation of the configuration of a stack.

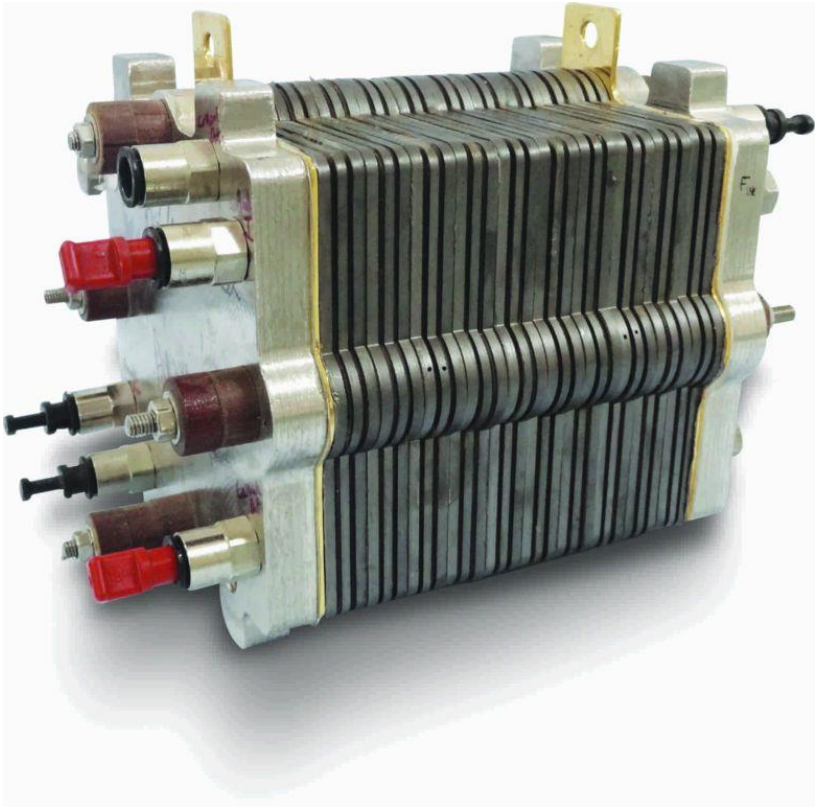

Figure 6. Fuel cell stack

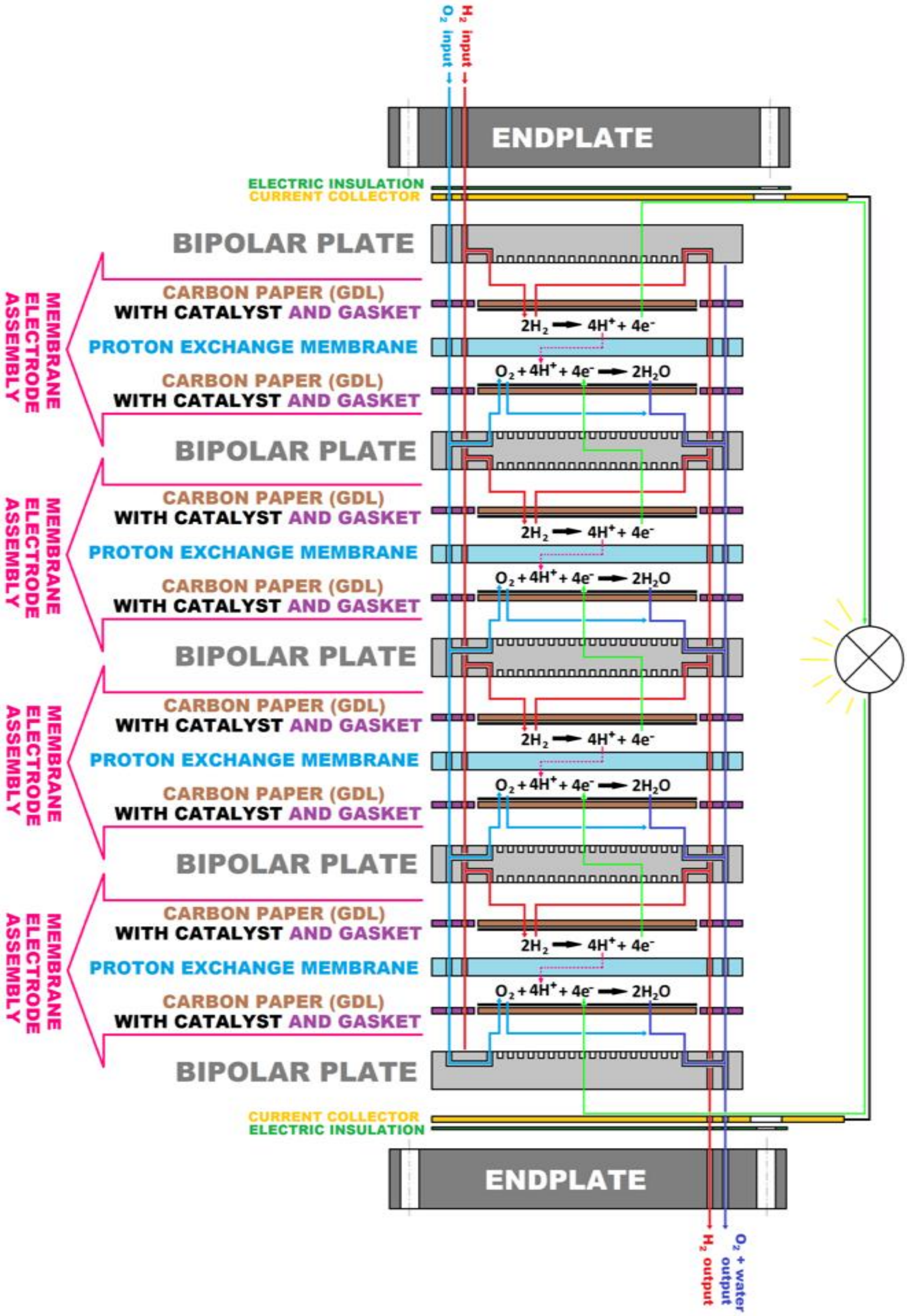

Figure 7. Demonstration of the configuration of a PEMFC stack

There are still some scientific challenges in the PEMFC technology and commercialization, such as: find anodic electrocatalysts that are tolerant to CO at levels of 100 ppm, the invention of a cathodic electrocatalyst to reduce the over-potential encountered at the open circuit to significantly enhance the exchange current density and find alternative proton conducting membranes with lower cost [1].

Another type of engineering approach for PEMFC is improving performance and overcoming model-based and data-driven limitations [36]. Besides that, the cost of the PEMFC due to the utilization of Pt as a catalyst is a challenge for reaching market potential of this technology. Pt is a noble and expensive metal, which increases the price of the PEMFC. Studies to reduce the overall Pt loading and find another type of catalyst is a material science issue. Now the goal is that the fuel cell stack of an FCEV has to contain a maximum as many noble metals as are contained in the catalyst of an Internal Combustion Engine (ICE) vehicle, with the same power range. In that case, technology will be rentable. ***Table 3*** shows the present state of the fuel cell requirements and the goal for the future. [37]

Table 3. PEMFCs is vehicles industry

	Nowadays	Goals for 2025
Pt content (g/kW)	0.35	0.10
MEA Power (W/cm^2 @ 1.5 A/cm^2)	0.75-1	1.5-1.8
MEA Power decrement (μV/h @ 1,5 A/cm^2)	22	11
Lifetime (h, in case of 10 % power decrement)	3000	6000
Power density (kW/kg)	2.3	3
(kW/liter)	3.5	5

PEM fuel cell operates at high efficiency and only generates water and heat as byproduct. That is why it is a promising alternative for fuel cells. The efficiency of the PEMFC is also related to the operating conditions of the system. The temperature, pressure, stoichiometry number has an essential influence on efficiency.

Degradation and stability are some of the challenges faced with PEM fuel cells. This is a barrier and reason for delaying PEMFC commercialization as the membrane is susceptible to physical and chemical degradation [6]. Stability is defined as how capable the fuel cell stack can resist permanent performance changes [6]. The degradation and stability are related to the cell's power output and the number of hours it can operate without drastic changes.

The degradation in the membrane assembly can be divided into reversible and irreversible degradation. The reversible degradation can be calculated as all the degradation that can be eliminated upon the membrane's regeneration whereas the irreversible one cannot be recovered. Irreversible degradation is the result of mechanical, chemical, and thermal degradation [6]. Mechanical degradation is related to the failures and cracks into the membrane, while chemical degradation is a damage and loss in PEM functionality resulting from chemical attack [6].

PEMFC has been used in many applications nowadays, it was used in aerospace, aircraft, automotive, and energy storage systems and it was the first type of Fuel Cell applied in NASA [1] [2]. Other researches on more applications of PEMFC has been made currently, for example, the use of a hybrid system combining proton exchange membrane fuel cell and supercapacitor to form a passive hybrid system [34]. In this hybrid system, the resistor was wired parallel with the PEMFC and connected through a contactor [34].

The representation of the diagram and picture of the system is shown in ***Figure 8***. In the diagram, contactors provide the electrical isolation between the fuel cell, supercapacitor, and load. In this system, a 9.5 kWe proton exchange membrane fuel cell is coupled with a 33 x 1500 F supercapacitor, and the results show that the system reduced dynamic loads on the fuel cell without additional DC/DC converters, and the fuel efficiency was increased by approximately 5% [34].

Europe manufacturer has announced the usage of PEM fuel cells in planes as a zero-emission passenger carrier (**Figure *9***). The ZEROe consists of 6 "pods" which act as standalone turboprop motors, 8-bladed propellers made of composite materials, removable fixtures along the wing for quick pod assembly & disassembly, and distribution hydrogen fuel cell system.

As mention previously, the PEM fuel cell was the first type of fuel cell used for aircraft application in NASA, and it has been used for many spacecraft since the Gemini program (***Figure 10***) [35]. PEM fuel cell has been used due to power output and water production capability long duration for the mass and volume. NASA Glenn Research Center is currently leading a PEMFC program to move the technology closer to the point required for space-flight purposes [35]. The Gemini fuel cell was rated near to 1kW and used spacecraft from 1965 to 1966.

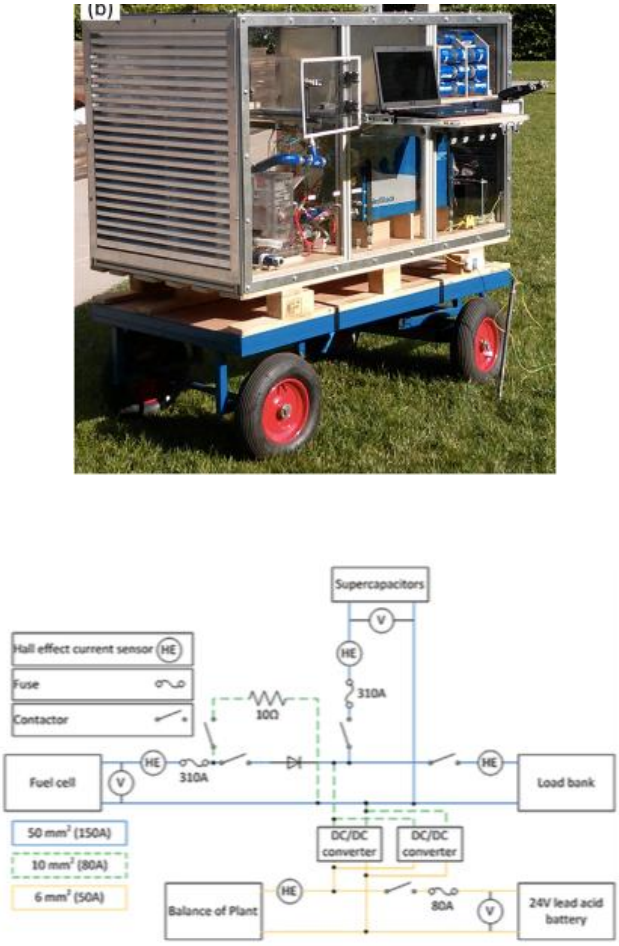

Figure 8. 9.5 kWe proton exchange membrane fuel cell is coupled with a 33 x 1500 F supercapacitor

Figure 9. ZEROe plane figure, a development from a European manufacturer in order to produce a zero-waste passenger carrier.

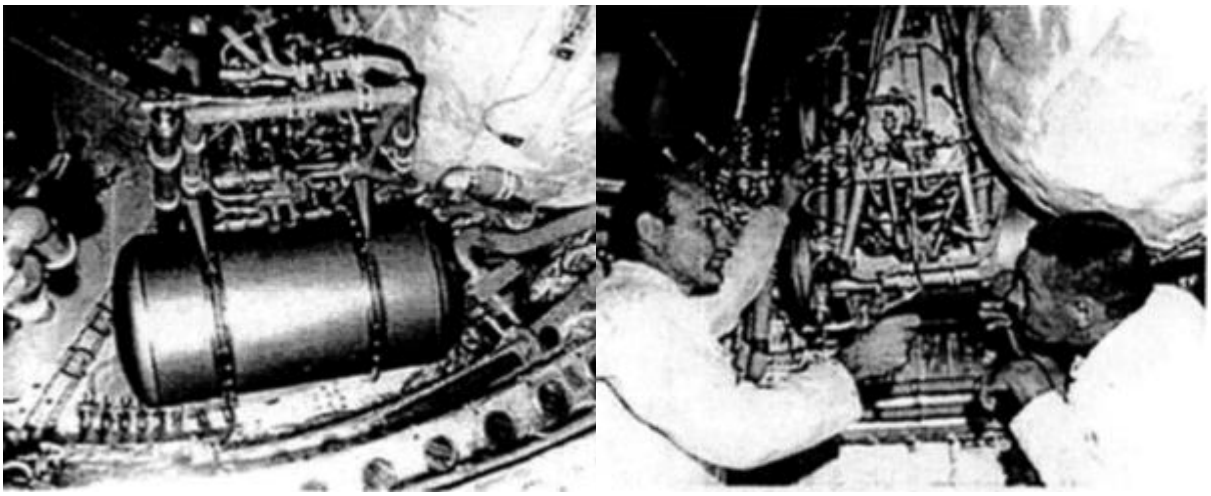

Figure 10. PEM Fuel Cell in Gemini 7 Spacecraft

2.4. CO tolerance of PEM fuel cells

Nowadays, the most significant amount of the world's hydrogen production is given by the oil refinery industry, with reforming processes. Because of the technology, the obtained hydrogen always contains a small amount of CO (1-2 V/V%), which can cause significant damages to the efficiency of PEMFC because CO adsorbs strongly on the catalyst surfaces, consequently blocking the adsorption sites for hydrogen [38]. PEMFC needs to deal with this drawbacks of the cost and durability for commercialization. It has very low tolerance towards impurities in the fuel [39]. The CO tolerance of PEM fuel cell has to be improved as CO contamination results in drop of the energy conversion efficiency. To minimize the contamination of CO in the fuel cell, it is crucial to purify the fuel stream before feeding it to the fuel cell to reduce the CO content to below less than 10 ppm [38]. There are several possibilities to deal with the CO contamination issues [40]:

- Optimization of the reforming of alcohols or biogas
- Addition of oxidizing agent to fuel
- Rising working temperature of the cell
    - PEM development for higher temperatures
- Development of CO tolerant electrocatalysts
    - Modification of active noble metal
    - Development of catalyst support/modification of active carbon
    - Development of noble metal-free electrocatalysts

The fundamental problem is the CO content of industrial hydrogen. The electrolysis of water can produce clean hydrogen from renewable electricity. Previously, high cost was the most crucial barrier against spreading renewable technologies; however, the remarkable improvement of the efficiency of photovoltaic (PV) panels induced a price drop in the last ten years. ***Figure 11*** shows this process graphically.

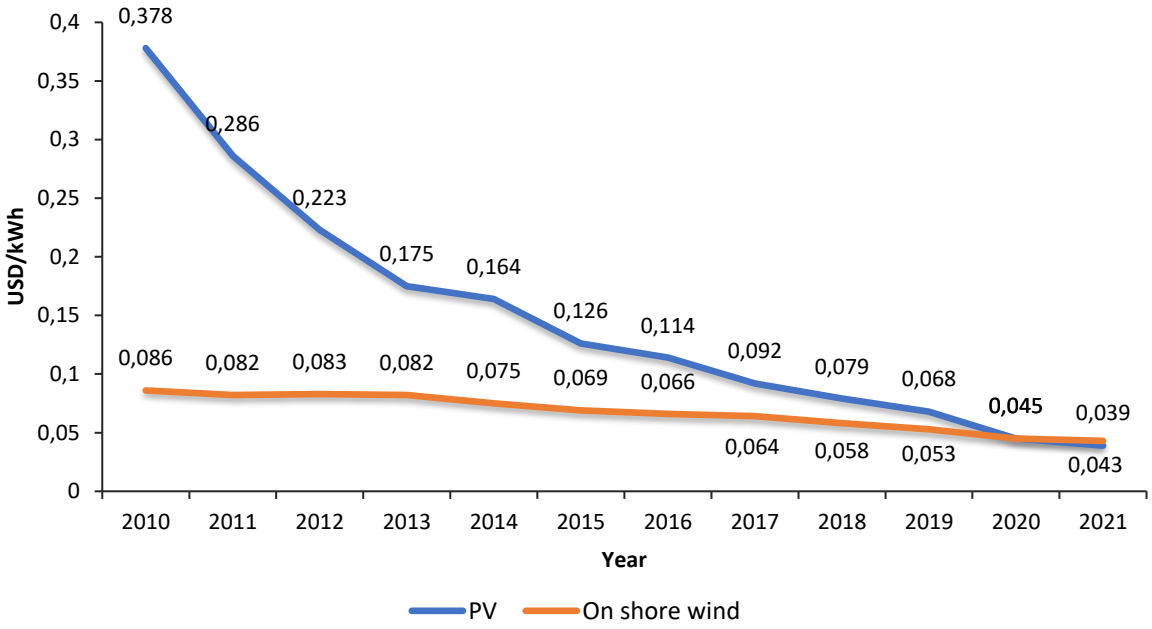

Figure 11. Price comparison (USD/kWh) of energy from photovoltaic (PV) and on-shore wind between 2010 to 2021 (adapted from How Falling Costs Make Renewables a Cost-effective Investment (irena.org)).

It is visible that nowadays, development of CO-tolerant fuel cells and the development of CO-free hydrogen production are two possible ways, and both have their importance.

2.5. Electrochemical Impedance Spectroscopy (EIS) in PEMFC analysis

Electrochemical Impedance Spectroscopy is a type of non-steady method which is based on imposing harmonic perturbation, by the application of small alternating voltage (potentiostatic EIS - PEIS) or current (galvanostatic EIS - GEIS), to the system and measuring the impedance under a various frequency [41] [42]. The EIS technique uses different frequencies and a frequency response analyzer (FRA) and load bank are required for the experiment [41]. The FRA sinusoidal wave produced is applied on the fuel cell via load bank, consequently, a system response is generated and an impedance spectrum is calculated [41]. In

summary, impedance is a type of measurement that analyze the ability of a system to impede the flow of electrical current, it is a powerful technique that can solve various polarization loss and it has been applied widely on PEMFC [42].

Impedance spectroscopy is widely used in electrochemistry due to its flexibility and accuracy [41]. The EIS has some application on the study of the fuel cell as temperature and humidity effects, sub-zero conditions, catalyst layer, gas diffusion and microporous layers, membrane, contamination, aging and durability, and dehydration or flooding. The current work the impedance spectroscopy was used to analyze the ionic conductivity of the membrane.

For the aim to correlate the Impedance Spectroscopy within the fuel cell, a novel 11-element impedance model of a PEM fuel cell was created (***Figure 12***). The figure shows a 1D description through the membrane and electrodes, however, the model does not analyze the variation of performance across the thickness of the electrode and along the length of the flow path [43].

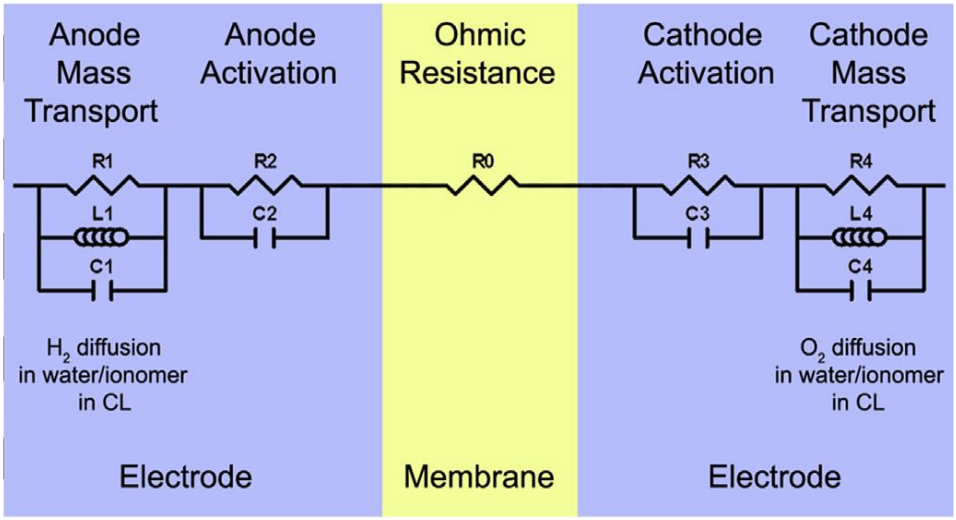

Figure 12 - A novel 11-element impedance model with an approximate schematic representation of the relationship between the fuel cell geometry and the proposed electrical equivalent circuit. (Pivac, I., Simic B., Barbir, F., 2017)

It is possible to simplify the 11-element impedance model since the impedance of the cathode is much higher than that of the anode (only N_2 goes to the cathode and therefore the speed of the electrochemical processes is lower, but its resistance is higher), and it not occur in the measured values and can be omitted. Parts R4, L4 and C4 can also be omitted from the scheme because no oxygen is applied to the electrode, the inductance element can be excluded by the fixed connection of the corresponding cable.

In the PEIS measurement the a steady-state perturbation is applied on the voltage and the response is recorded ***Figure 13***. The current is the response and it has variational phase and amplitudes.

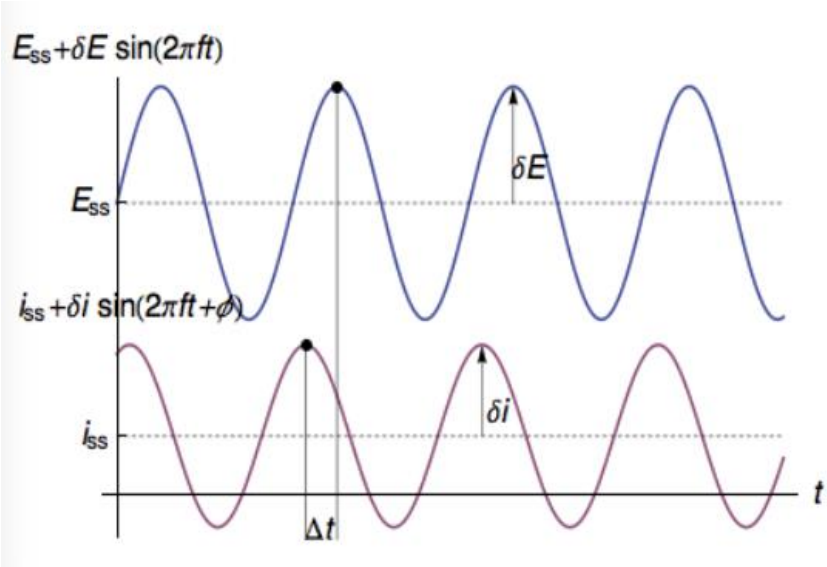

Figure 13. The Impedance measurement based on the study of the response of a system subjected to sinusoidal potential (or current) modulations of various frequencies.

The impedance is a complex number in which:

$$Z = a + jb = Re(Z) + jIm(Z) \qquad \textbf{Eq. 10}$$

$$Z = \rho(cos\phi + isin\phi) \qquad \textbf{Eq. 11}$$

In which is possible to analyze the results through two different models the Bode and the Nyquist plot. In the Bode Plot, the modulus and the phase of the impedance are plotted against the frequency of the modulation, ***Figure 14a*** shows the DN021 Bode Plot. While in the Nyquist plot, the impedance for each frequency is plotted in a complex plane -Im(Z) vs. Re(Z), ***Figure 14b*** shows the DN021 Nyquist plot.

It is possible to deduce Bode from Nyquist by the Pythagorean theorem:

$$IZI = \sqrt{Re(Z)^2 + Im(Z)^2} \quad \varphi z = arctan\frac{Im(Z)}{Re(Z)} \qquad \textbf{Eq.12}$$

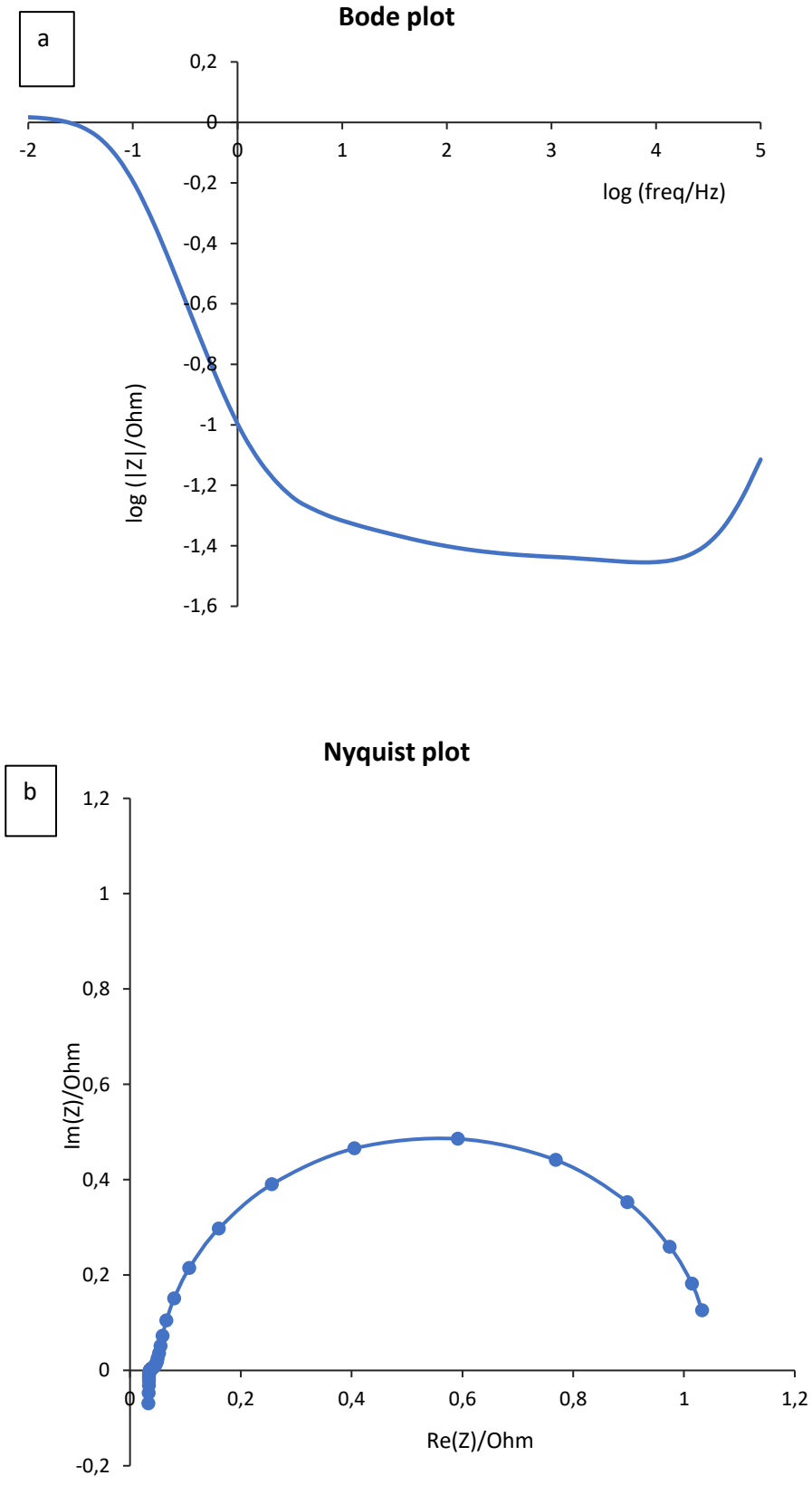

Figure 14. PEIS plot for DN021. a) Bode plot. b) Nyquist plot

The processes taking place at the cathode and anode of the fuel cell can be well distinguished in the impedance spectrum. The Bode diagram in ***Figure 15*** below illustrates the typical frequency bands where diffusion in solution and electrocatalyst layer, oxygen reduction-related electrochemical reaction (ORR) and hydrogen oxidation processes (HOR) and membrane and electrical resistance of catalyst layers.

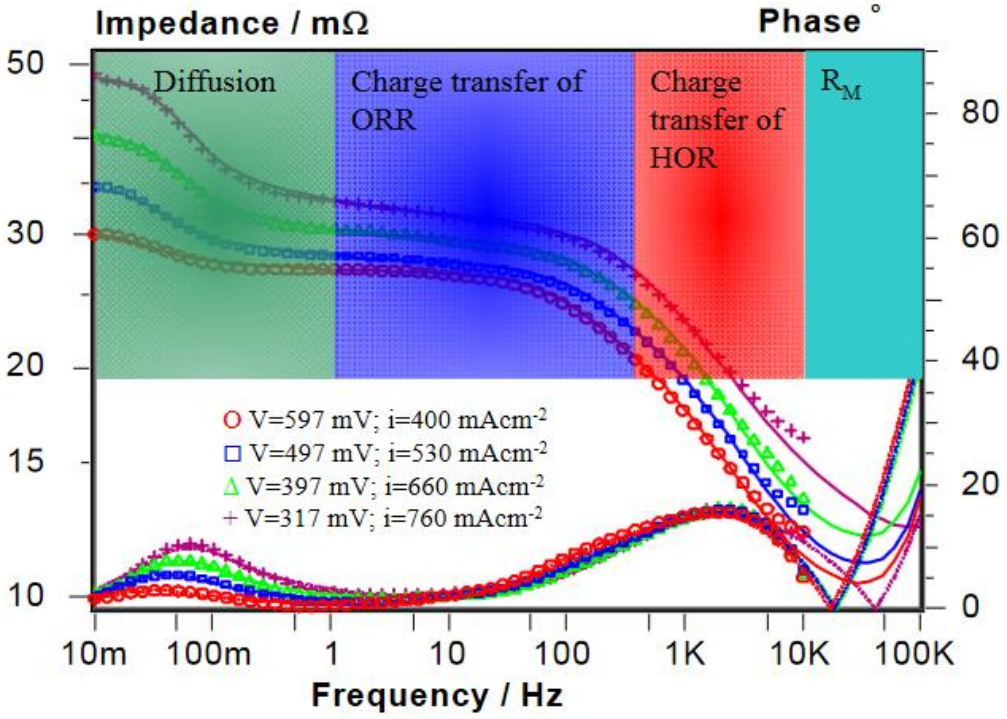

Figure 15. Bode representation of EIS measured at different current densities, PEFC operated at 80ºC with H_2 and O_2 at 2 bar (N. Wagner, from PEM fuel cell diagnostic tools, 2011)

Model circuit of the electrochemical processes of the analyzed system can be simplified, as ***Figure 16*** shows. R_Ω is the ohmic resistance (the resistance of the cell). This is in connection with the conductivity of membrane, but conductivity of catalyst layers of MEA also belongs to this value. Because of that, if R_Ω changes by the composition of applied catalyst layer, the change will belong to the catalyst layer, because conductivity of membrane theoretically will not change. Electrode impedance has a Faradaic and a non-Faradaic part. Faradaic impedance (usually the polarization resistance R_{ct}) belongs to the electrochemical reaction. In that impedance M is a so-called Wartburg impedance, which belongs to material transport, in case

of the presence of ion diffusion, which slows the processes. Non faradaic component obtained from the double layer capacitance, because interface is able to work as capacitor by adsorption of ions on the surface of the electrode. This results the charging of the formal capacitor, and that interfacial capacitor is called double layer capacity (C_{dl}). Increment of Cdl shows, that real surface of the electrode increased or it became porous. Because of that, changing of C_{dl} gives information about the size and the roughness of the surface of electrode.

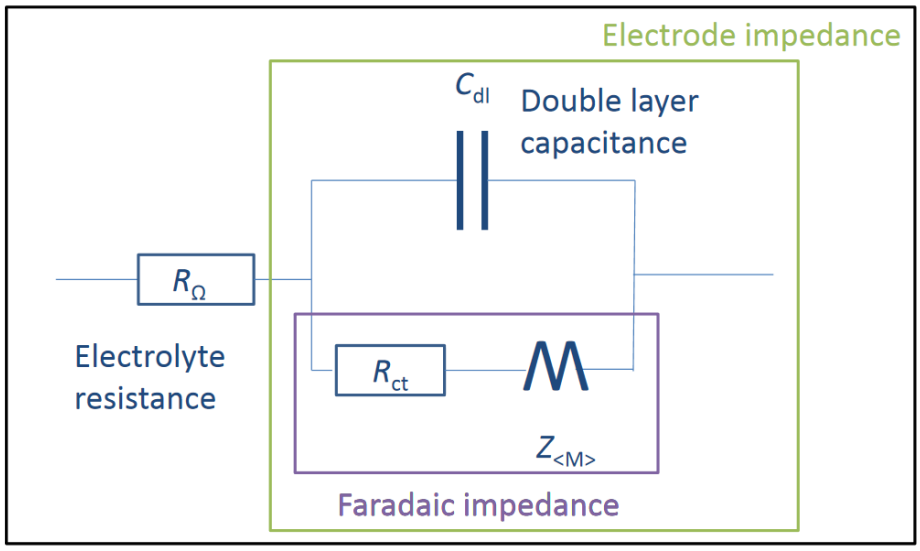

Figure 16. Simplified model circuit of electrode processes

3. Aim of the study

My goal was to establish and validate the methodology for MEA testing in the research group. Project consists of the following steps: i.) make experimental MEAs with a method, which is suitable for laboratory scale, ii.) measure them according to an internationally used protocol, iii.) optimize the Pt loading of MEAs, iv.) make MEAs with application of those catalyst supports, which were developed in our research group, v.) carry out electrochemical characterization of catalysts and MEAs and evaluate the results, vi.) scale up the system. The applied strategy in order to accomplish the above goals was as follows:

i.) Configuration of spray coating of GDLs

Previously screen-printing method was applied for manufacturing of GDEs in the research group. Advantage of spray coating is that this is a quick method (1.5h vs. 24 or 48h) and easy to control. For laboratory scale this is a good technique, because GDE can be painted from small amount of catalyst (15 mg is enough for a 4x4cm GDL). SEM analysis was applied for checking the quality of spray coating.

ii.) Configuration of the measuring protocol.

For FC measurements a current, internationally applied method had to be found for obtaining comparable results to other researchers, who also work on this scientific area. The New European Driving Cycle (NEDC) is a suitable protocol for our measurements, because it describes exactly the measuring conditions and it contains methods for determination of the degradation of MEA and for analysis of working parameters. Last, but not least, this is an EU standard protocol, which is developed for testing of the MEAs of fuel cell vehicles.

iii.) Optimization of the Pt loading of MEA

For optimization of Pt loading, it is important to know, that nowadays in commercial fuel cells Pt loading is 0.35 gPt/kW and 0.1gPt/kW value should be reached until 2025. The goal was to reach or approach these numbers. MEAs were planned with different Pt loading, from 0.05 to 0.2 mgPt/cm^2, with the same noble metal content on both sides of the MEA. After the

optimal loading had been found, new MEA was be made with decreased Pt loading on anode. In that stage of optimization, only commercial reference catalysts were applied.

iv.) Testing of different anode catalyst supports in FC measurements

Next step was to make MEAs with those catalyst supports, which were developed in the research group. Different $Ti_{0,8}Mo_{0,2}O_2$-C composite supports were platinated, examined and used for anode catalysts. Their preparation method and characterization were the subject of a previous MSc theses (Kristóf Zelenka) in the research group. In these composites variable was the type of applied carbon (Black Pearls, functionalized Black Pearls and Vulcan). These supports have not been examined previously in real fuel cell measurements. The goal was the addition of Pt to the supports, MEA making from these ready catalysts according to the results of iii.) and then the FC testing of these MEAs, according to the NEDC protocol, which was configurated in ii.)

v.) Electrochemical characterization

In that chapter there were two separated parts. Firstly, applied anode catalysts were examined in a 3-electrode cell, on rotating disc electrode (RDE), for measuring hydrogen oxidation reaction (HOR) and compare them to each other. Second part was the direct electrochemical characterization of MEAs in the fuel cell. Connection of the FC tester and a multichannel potentiostat let us to carry out cyclic voltammetry (CV) measurements from the MEA and to measure potentiostatic electrochemical impedance spectroscopy (PEIS). Results of these analysis helped us to understand and determine the different surface processes of the fuel cell.

vi.) Scaling up of the cell

Measurements were carried out in a 16 cm^2 active area fuel cell. The goal was to make a 50 cm^2 cell and compare the results. Scaled up cell was designed in our research group, in collaboration with the Department of Polymer Technology (Technical University of Budapest) and with H-ION Ltd. Polarization curves, and voltammograms were compared.

4. Experimental

4.1. Preparative methods

4.1.1. Preparation of catalyst support

That step was not the part of my work and practically it was not the first step of the process. Although these things, it is necessary to describe this process, because according to the logical sequence, that should be the beginning. On the other hand, "Optimization of anode catalysts" chapter cannot be understood without that part.

Applied catalyst supports were previously developed and made in our research group by Kristóf Zelenka, according to the following description [44]: Titanium-isopropoxide ($Ti(OCH(CH_3)_2)_4$) was added drop by drop to water solution of nitric acid under vigorous stirring. After that, reaction mixture was stirred for 4 hours on room temperature, then active carbon was added, which was previously suspended in water by ultrasonic shaking. After that, the whole carbon containing mixture was stirred for 4 days on room temperature, then molybdenum precursor $(NH_4)_6Mo_7O_{24}\cdot 4H_2O$ was added to this. Finally, solvents were evaporated form the sample under mixing on 65°C, then material was dried and heat treated on high temperature and inert atmosphere (600°C, 8h, Ar). The ready support contained 25% of $Ti_{0,8}Mo_{0,2}O_2$, and 75% of carbon.

Variable was the type of applied active carbon. CABOT was the manufacturer and the used carbons were the Black Pearls 2000 (BP) and the Vulcan XC-72 (Vul). In case of functionalized Black Pearls (F*BP) surface of carbon was treated in 3M HNO_3, then it was washed to neutral pH and water-ethanol solution of glucose was added to this. That mixture was shaked for 2 hours on RT. These materials were previously characterized, but they were not examined in HOR, DLC and PEIS measurements. ***Table 4*** contains the abbreviation of the catalysts, which were based on these supports and which were platinated with 20m/m% Pt, according to the next chapter.

Table 4. Abbreviation of carbon – mixed oxide supported catalysts, used in this project

Abbreviation	Exact composition
Pt_TiMoO2-BP	20 wt.% Pt – (25 wt.% of $Ti_{0,8}Mo_{0,2}O_2$ mixed oxide and 75 wt.% BlackPearls 2000 active carbon)
Pt_TiMoO2-F*BP	20 wt.% Pt – (25 wt.% of $Ti_{0,8}Mo_{0,2}O_2$ mixed oxide and 75 wt.% functionalized BlackPearls 2000 active carbon)
Pt_TiMoO2-Vul	20 wt.% Pt – (25 wt.% of $Ti_{0,8}Mo_{0,2}O_2$ mixed oxide and 75 wt.% Vulcan XC-72 active carbon)

4.1.2. Addition of Pt to catalyst support

The platinum addition to the catalyst support was made by using $Ti_{(1-x)}Mo_xO_2$-C composite materials and loaded with 20 wt.% Pt via modified $NaBH_4$ – assisted ethylene-glycol (EG) reduction-precipitation method [45].

In all cases, $H_2PtCl_6 \cdot 6H_2O$ was solved in 50ml of ethanol, and 200mg of the sample was suspended in the solution. A solution prepared by mixing $NaBH_4$ and EG was added dropwise to the suspension at 65°C with continuous stirring. After 3 hours of stirring at 65 °C, HCl is added to the suspension and stirred for an additional 2.5 hours at room temperature to deposit the Pt particles onto the support material. The materials were washed three times with 50 ml water and filtered by centrifugation in order to remove the chloride ions and dried at 80 °C in an oven overnight. The whole platination process can be seen on ***Figure 17***.

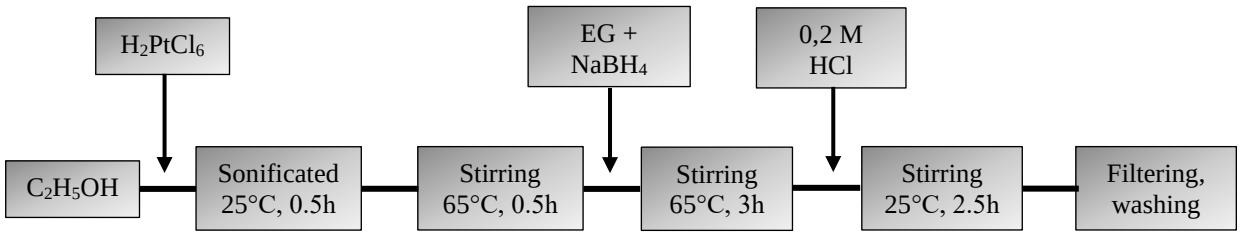

Figure 17 – Flowsheet image of the steps and times for addition of platinum to the support.

4.1.3. Membrane electrode assembly preparation protocol

Fuel cell testing measurements were carried out on an FCT-150S apparatus by BioLogic. QuinTech C-20-PT was used as a reference catalyst, with 20 m/m% Pt content. Other components of the catalyst ink were Quintech NS05 nafion solution (5 m/m%) and a.r. 2-propanol (99.99 V/V%, Molar Chemicals Kft.). Catalyst ink was painted onto the surface of the GDE by spray coating method. For this method, AB200 type airbrush was applied from Conrad Electronic SE.

Catalyst ink composition was obtained by more optimization steps. Variable parameters were the catalyst: ionomer ratio, the type and amount of solvent, Pt content of catalysts, Pt loading of GDEs, mode of the homogenization of catalyst ink, and the calculated loss. The mass ratio of the catalyst to dry Nafion is 2:1. The solvent is isopropanol which is applied in the same volume as Nafion solution. Previously water was applied as solvent, but the evaporation speed was lower than in isopropanol, and the surface of GDEs was not so even. The calculated loss is 60%. A detailed receipt is introduced in ***Table 5***.

Table 5. Catalyst ink composition for spray coating of GDEs

Parameter	**amount**	**unit**
Surface	32	cm^2
Pt density	0.05	mg/cm^2
Pt content of catalyst	20	%
Nafion content of Ionomer	5	%
calculated loss	60	%
d Nafion solution	0.938	g/ml
mass rate of dry nafion to cat.	0.5	-
m cat.	**20.00**	**mg**
V Ionomer	**0.213**	**ml**
V solvent (a.r. isopropanol)	**0.213**	**ml**

Two GDEs had been parallelly made because cathode and anode have the same Pt content ($0.05mg/cm^2$) in the MEA preparation optimization stage. After that, they were heat-treated in the air for 30 minutes at 70°C, then for additional 30 minutes at 125°C. For getting a ready MEA, cathode side GDE, Nafion membrane, and anode GDE were pressed together with 57.3 kg/cm^2 pressure for 3 minutes, on 120°C.

4.2. The fuel cell workstation

Measurements were carried out in a complex workstation, in which a fuel cell tester (BioLogic FCT-150S), and a multichannel potentiostat (BioLogic VMP-300) were connected to a measuring computer through a switch, as a local area network. In case of fuel cell measurements (NEDC protocol and Pmax determination; see later), FC tester is regulated by the FC-Lab program (the original program of the apparatus). If CV or PEIS measurement is carried out on the fuel cell, FC tester provides the gas flow and temperature control, but the measurement itself is controlled by the potentiostat, with EC-Lab program. In that case two system is in parallel connection. ***Figure 18*** shows the workstation.

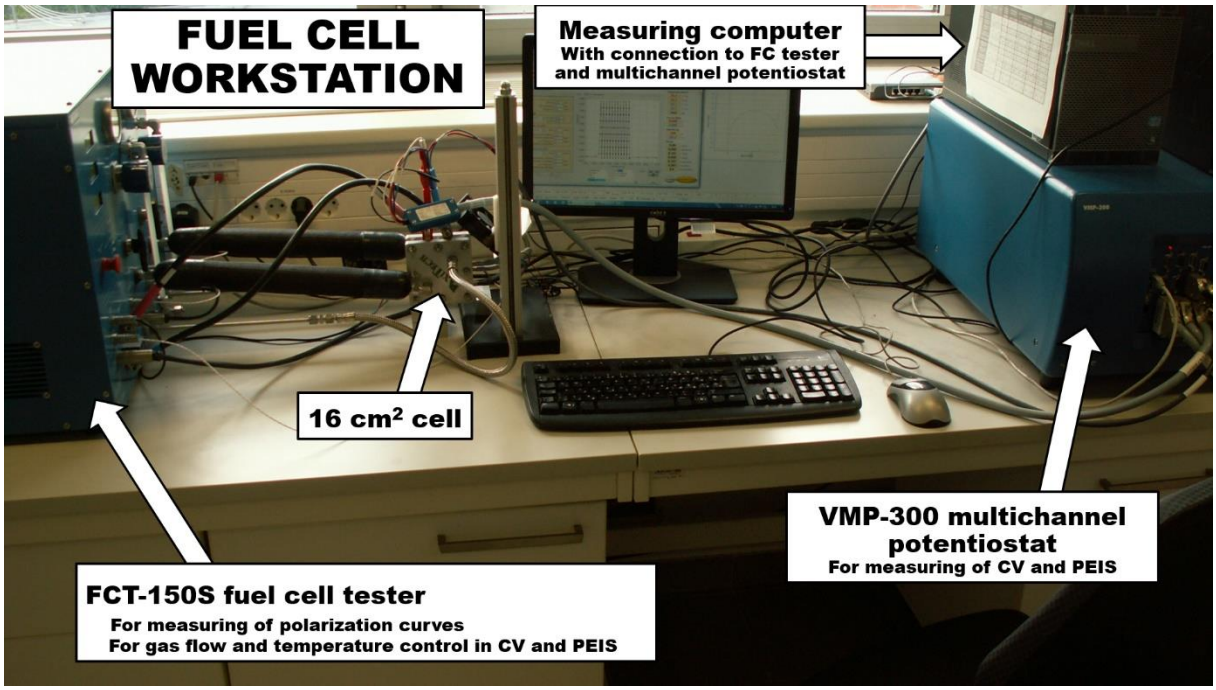

Figure 18. The applied fuel cell – potentiostat complex workstation

4.3. Measuring methods

4.3.1. MEA characterization before FC testing

In optimization of MEA preparation, quality control of airbrush technique was necessary to know, that is the applied method suitable or further development is required. Firstly I applied Digital Microscope Camera (TOOLCRAFT) with 50x zoom to check the surface of ready GDE. Preliminary experiments showed, that if spray coated surface was even, smooth and not cracked, GDE was suitable for making MEA from it. ***Figure 19*** shows the

difference between uncoated and spray coated carbon paper (uncoated part was the fixation point under spray coating).

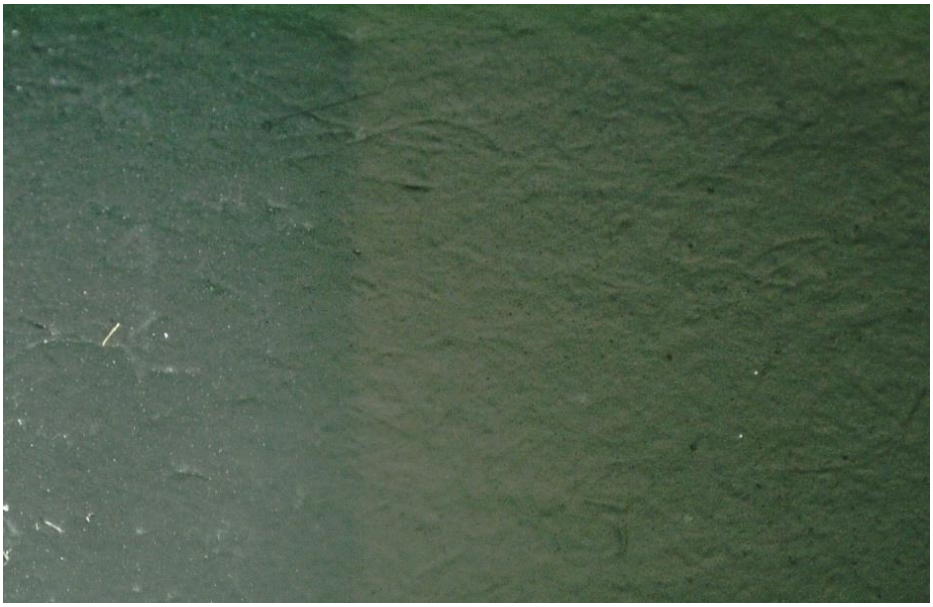

Figure 19. Uncoated and spray coated parts of GDE, before it was cut to size. Image was taken by Digital Microscope Camera, with 50x zoom

Energy-dispersive X-ray spectroscopy let us to take Pt elemental map from the surface of GDE. This method is able to show appearance of the inhomogeneities of painting after application of airbrush. For analysis 9 different 3x3mm window was scanned on the GDE, according to **Figure *20***. Pt loading of GDE was 0.05mg/cm^2 and the applied catalyst was Quintech C-20-PT. Measurement was carried out in the laboratory of H-ION Kft.

For study of the surface morphology of the MEA and GDE, two samples were analyzed with scanning electron microscopy (SEM). First was a GDE with 0.05mg/cm^2 Pt loading, and the second was a ready hot-pressed, but not applied MEA, with 0.05mgPt/cm^2 on both sides. 1000x scale image was taken from the GDE. MEA was cut and 400x scale image was taken from the section. These analyses were carried out in the laboratory of National Institute of Material Phisics (Romania).

Figure 20. Arrangement of EDS scanned windows on the surface of ready GDE.

4.3.2. NEDC protocol

Testing of MEAs was carried out according to the New European Driving Cycle protocol (NEDC). The purpose of these measurements is to make a laboratory simulation of real driving conditions. The procedure will be detailed in the following. The most important steps of MEA testing are: i.) Activation of MEA, ii.) Taking of polarization curve to determine the 100% loading, iii.) Running of Dynamic Load Cycle (DLC) test (16.4 h), iv.) Taking of polarization curve after DLC test, v.) Regeneration of MEA (16.4 h), vi.) Taking of polarization curve after MEA regeneration.

4.3.2.1. Activation of the MEA

Table 6 introduces the exact conditions of activation. Adjustments of activation and polarization were the same. In the first case, the voltage was held at 600 mV for six hours. The current needs to be risen and then stabilized under the time of activation.

Table 6. Conditions of activation and polarization

Parameter	amount	unit
T cell	80	°C
T H_2 line	85	°C
T H_2 humidifier	64	°C
H_2 rel. humidity	50	%
p H_2	2.5	bar
F H_2	200	ml/min
T O_2 line	85	°C
T O_2 humidifier	54	°C
O_2 rel. humidity	30	%
p O_2	2.3	°C
F O_2	200	ml/min

4.3.2.2. Polarization curve

The current has been changed according to a determined program in the polarization curve, which usually means stepwise rising. According to other methods, current would be stepwise increased and then decreased – NEDC polarization belongs to these methods. Voltage is the measured parameter, and the polarization curve shows the (decreasing) voltage as a function of current density (calculated from current and MEA surface). Current program of NEDC polarization is graphically visualized in ***Figure 21***. In this program, the current density has risen to 2 A/cm^2 in 16 steps, and then it is decreased to 0 in also 16 steps. A program step holds the current for 2 minutes, except the first and last six steps, which is only 1 minute.

When the polarization curve has been taken, the voltage must not decrease below 400 mV, according to the NEDC protocol. For this, the polarization program needs to be changed by skipping those steps, where current density is too much (which causes too low voltage). This is also visualized in ***Figure 21*** (see curves of SZG007 MEA). In the measurement technical aspect it means, that in this case, two polarization curves have to be taken. The current density maximum of the first polarization is 2 A/cm^2 (the original program). This program cannot run entirely, but it will show the most significant current density, where voltage is above 400 mV. That defined current density will be the j_{max} in the second polarization, and the results of that curve need to take into account in further calculations.

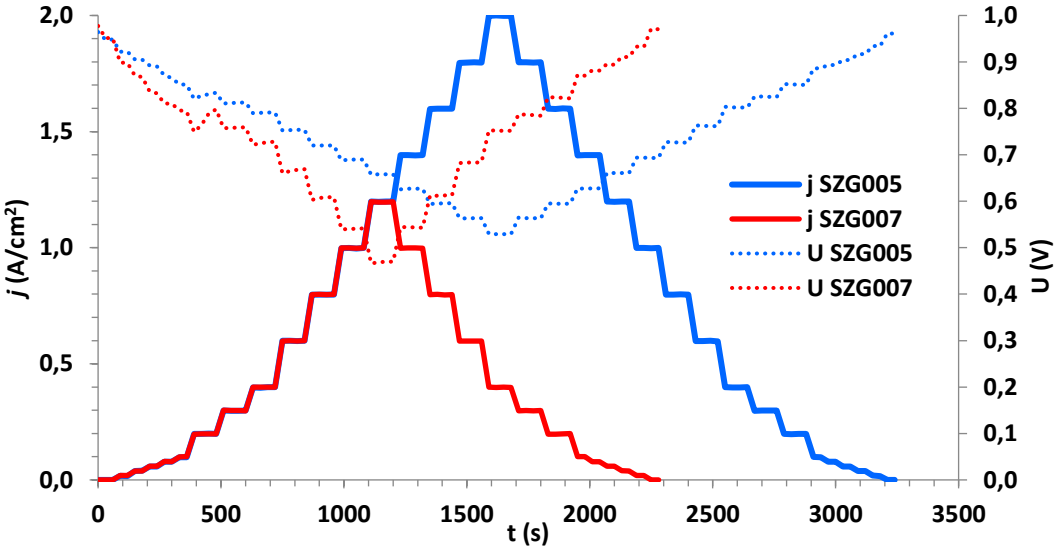

Figure 21. Graphical visualization of the polarization program, which was applied before and after the FC-DLC test. The figure shows that case (SZG007), where j_{max} had to be decreased.

As ***Figure 22*** shows, the result of the measurement is two curves, taken in ascending and descending current densities. This measurement's importance is the following: An arithmetic average of current densities, which belongs to the 650 mV (from ascending and descending curve) determines the 100% loading for the Dynamic Load Cycle test.

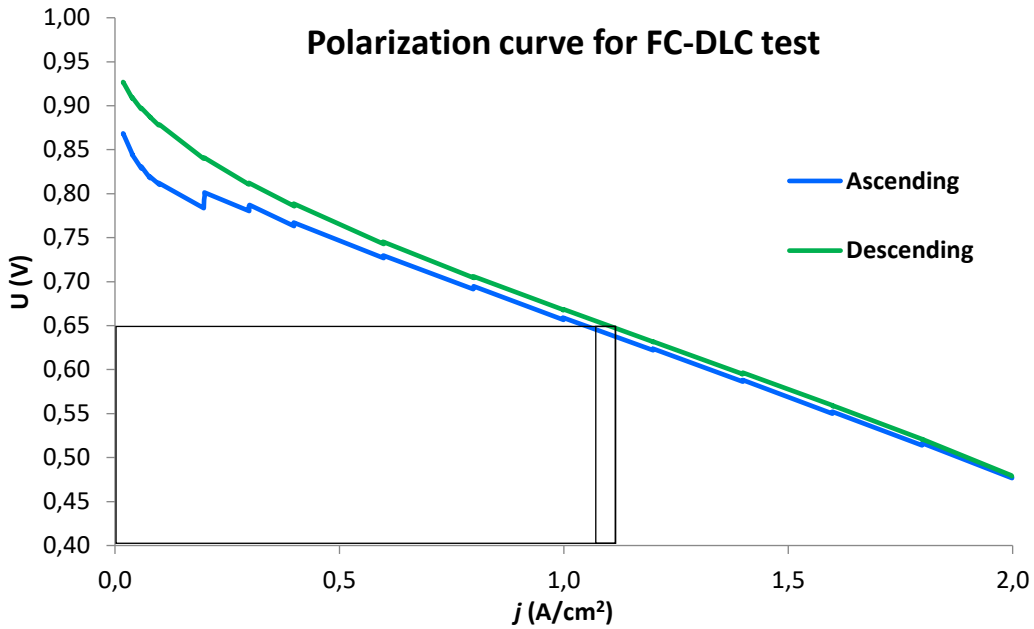

Figure 22. Polarization curve for FC-DLC test and determination of the current density of 100% loading

4.3.2.3. Validation of FC-DLC test and regeneration

The DLC test assesses fuel cell durability during a relatively long period by repeatedly exposing the cell to the same load cycle. The Fuel Cell Cycle is based on the NEDC protocol and, this is depicted in ***Figure 23***. The NEDC cycle is used for type approval of light-duty vehicles and features periods of acceleration, deceleration, and constant speed. It consists of four repetitions of a low-speed urban cycle of 195 seconds (grey line on ***Figure 23***), each followed up by a part that simulates a motorway (highway) driving cycle of 400 seconds duration. That is equivalent to a theoretical distance of approximately 11 km driven in about 20 min.

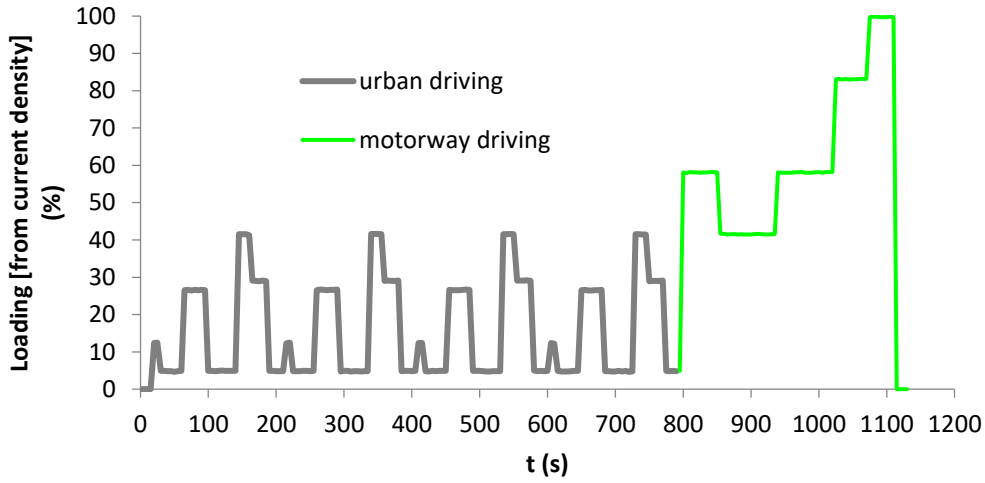

Figure 23. Graphical visualization of a cycle of Dynamic Load Cycle test.

The current density of 100% loading was calculated from the polarization curve, as it was previously detailed. The NEDC protocol gives percent loading as a function of time, so the current density program of the cycle depends on the polarization result. The same program is introduced in ***Table 7***. When the DLC test is carried out, the fuel cell cycle (***Figure 23***, ***Table 7***) is continuously repeated 50 times (16.4h) which is called "testing block". The 50 cycles "testing block" is theoretically equivalent to 550 km driving, the average range of a car after tanking.

Table 7. Program of the measurement cycle of DLC test

Number of program step				Length of program step (s)	Loading* (%)
0**				15	0
1	8	15	22	13	12.5
2	9	16	23	33	5
3	10	17	24	35	26.7
4	11	18	25	47	5
5	12	19	26	20	41.7
6	13	20	27	25	29.2
7	14	21	28	22	5
			29	58	58.3
			30	82	41.7
			31	85	58.3
			32	50	83.3
			33	44	100
			34	21	0

* Calculated from the average current density on 650 mV
** Program of FCT apparatus starts the steps from 0

The polarization curve needs to be retaken after finishing the 50 cycles, and then MEA will be regenerated. The time of regeneration is the same as the testing block. The cell has been purged with N2 under working temperature and pressure until the opened circuit voltage decreases below 20 mV. If cell voltage small enough, gases will be changed to O_2 both on cathode and on anode side, and the cell will be cooled down to room temperature in O_2 flow. The last step of the regeneration is that pressure is let down, flows will be closed and the cell has been left at room temperature for 16.4 h. The complete stability testing plan of NEDC protocol contains 1400 cycles, i.e. 28 testing blocks, which is equivalent to the annual stressing of the cell stack of a fuel cell vehicle.

4.3.2.4. Determination of rate of degradation

The efficiency of the MEA will be decreased at the end of DLC test, as is visible in ***Figure 24***. This situation has been creating question to the researchers if, in case of regeneration, it would be possible for the regeneration to be increased back to the starting conditions.

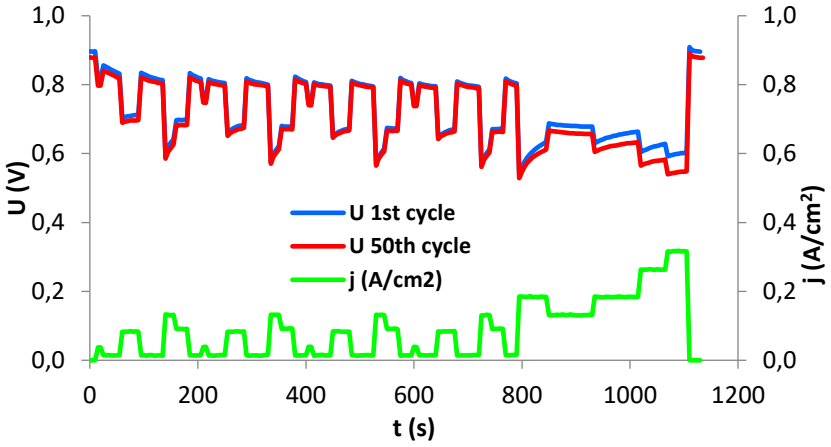

Figure 24. Comparison of the first and last cycle of FC-DLC test

Calculation of the degradation rate can answer this question. At the end of the DLC test and the regeneration, the result will be three polarization curves: before the DLC, after the DLC, and after the regeneration. These curves are introduced in ***Figure 25***. In all cases, only the descending part of the polarization curve was visualized on the graph. If degradation is calculated, voltages of the current density maximum will be taken into account. Unit of the degradation is µV/h. According to the rate in which regeneration restores the beginning conditions, degradation has reversible and irreversible parts.

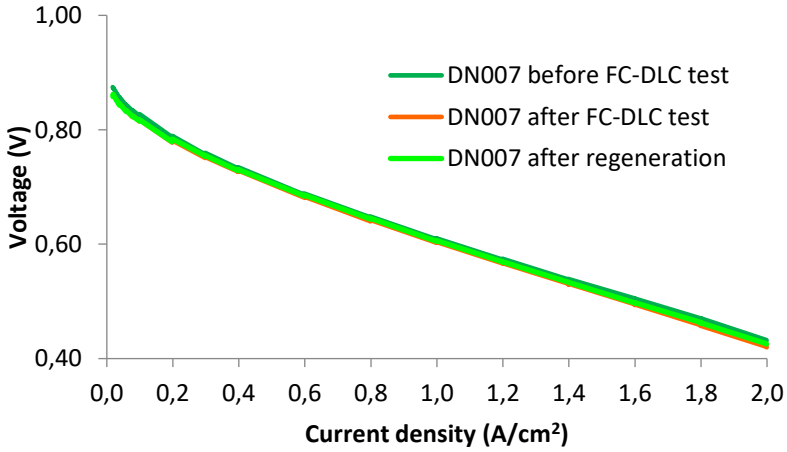

Figure 25. Polarization curves before DLC test, after DLC test, and after regeneration (for calculation of degradation)

For better understanding, ***Figure 26*** schematically introduces the amounts necessary for the calculation of degradation.

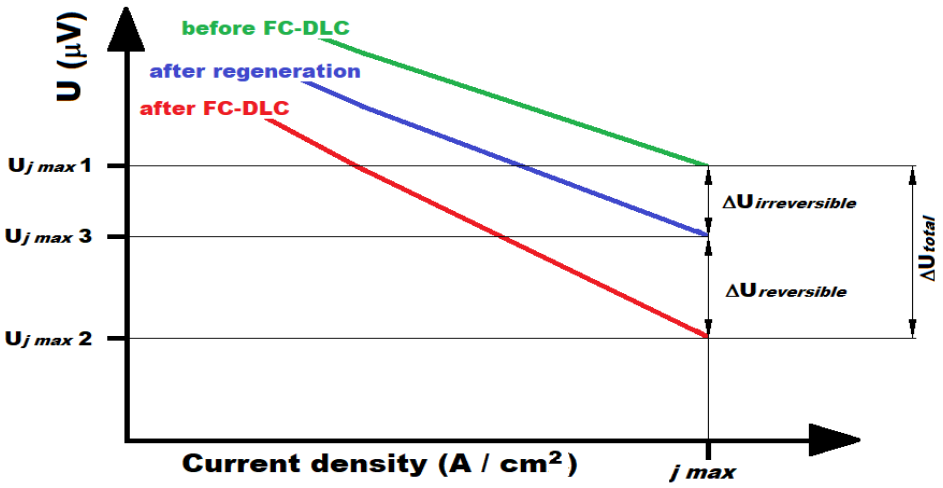

Figure 26. Schematic visualization of the amounts for the calculation of degradation, obtained from polarization curves

The most important parameters are the time of a testing block (16.4 h; time of 50 DLC cycles) and those voltages, which belong to the current density maximum (j_{max}) of polarization curves before FC-DLC (Ujmax1), after FC-DLC (Ujmax2), and after regeneration (Ujmax3). Unit of voltage is µV for calculation of degradation. Voltage differences (reversible, irreversible, and total are DU, but they are signed as DV in NEDC protocol. Total degradation is the sum of reversible and irreversible degradation.

Formulas of calculation of the degradation are the following (Eq. 10-13):

$$\dot{V}\text{total}\left(\frac{\mu V}{h}\right) = \frac{\text{Ujmax1}(\mu V) - \text{Ujmax2}(\mu V)}{\text{t testing block (16.4 h)}} = \frac{\Delta\text{Utotal}(\mu V)}{\text{t testing block (16.4 h)}} \qquad \textbf{Eq. 10}$$

$$\dot{V}\text{reversible}\left(\frac{\mu V}{h}\right) = \frac{\text{Ujmax3}(\mu V) - \text{Ujmax2}(\mu V)}{\text{t testing block (16.4 h)}} \qquad \textbf{Eq. 11}$$

$$\dot{V}\text{irreversible}\left(\frac{\mu V}{h}\right) = \frac{\text{Ujmax1}(\mu V) - \text{Ujmax3}(\mu V)}{\text{t testing block (16.4 h)}} \qquad \textbf{Eq. 12}$$

$$\dot{V}\text{total}\left(\frac{\mu V}{h}\right) = \dot{V}\text{reversible}\left(\frac{\mu V}{h}\right) + \dot{V}\text{irreversible}\left(\frac{\mu V}{h}\right) \qquad \textbf{Eq. 13}$$

Degradation can be calculated in case of more testing blocks (up to 28); in this study, the case of one testing block (50 cycles; 16.4 h) – one regeneration was analyzed.

4.3.3. Determination of Power maximum

That measurement was made on every MEA of the project; the goal was to determine the maximum power reach for the MEA. The measuring protocol was an increase of 400mA every 60 seconds until voltage decreases bellow 200 mV. In case of NEDC polarization, the lower voltage limit is 400 mV. In that case it is too much, because MEA will not reach the power maximum, if measurement is stopped on that voltage. On the other hand, descending part of polarization curve is unnecessary in this case. These were the reasons of the changing of the polarization program. ***Figure 27*** shows a representation of the graph of power maximum for MEA DN018 as a function of current density (A/cm^2).

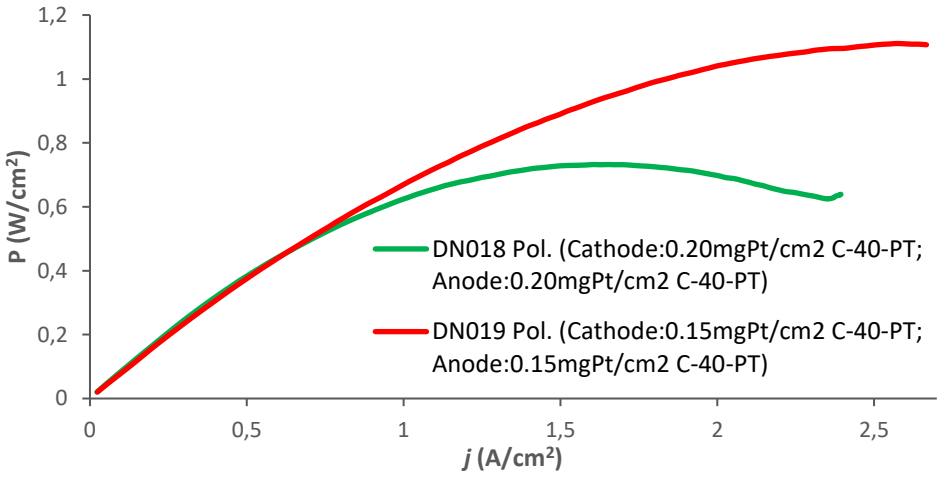

Figure 27. Graph visualization of determination of power maximum (W/cm^2) for DN018 and DN019 based on the current density *j* (A/cm^2)

4.3.4. Cyclic voltammetry (CV) measurements

Cyclic voltammetry is an electrochemical method, where potential of working electrode is changed with even pace (usually 10 or 100 mV/s according to the measuring mode) between two fixed voltage values (E1 and E2) there and back and these cycles can be repeated. In cyclic voltammetry current is detected as a function of potential. In my thesis two different cases were analyzed. First was the classic 3 electrode system (see below) and the second was the CV measurement on fuel cell (detailed later).

4.3.4.1. CV measurements on rotating disc electrode (RDE)

These measurements are carried out in 3 electrode electrochemical cell, which can be seen on ***Figure 28*** [44] [46]. All the applied electrodes were the products of ALS Inc. Reference electrode were the reversible hydrogen electrode (RHE), counter electrode was a Pt wire, and the working electrode was a 3 mm diameter (A=0.0707cm^2) glassy carbon rotating disc electrode (RDE). A BioLogic SP-150 potentiostat was used for these measurements, with EC-Lab program.

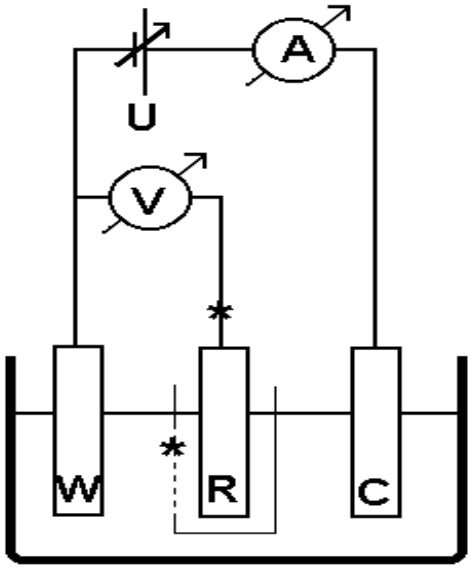

Figure 28. Scheme of 3 electrode electrochemical cell. W is the working electrode; R is the reference electrode and C is the counter electrode. Applied electrolyte was 0.5M H_2SO_4 solution.

For CV measurement catalyst ink was made from 2 mg of catalyst and 2 ml of Nafion-water-isopropanol solution according to the following ratio: 8µl of 5 m/m% DuPont Nafion solution, 400 µl of a.r. isopropanol and 1592 µl of 18.2 MΩ∗cm MilliQ water. Ink was ultrasonicated for 30 minutes before application. RDE was polished with suspension of 10µm grain size Al_2O_3 (by Nanografi) and isopropanol. 3.6ml of catalyst ink was dripped onto the surface of the electrode and then it was dried for 20 minutes. Applied electrolyte was 0.5 M H_2SO_4 solution. 3 electrode cell was applied in CV measurement for quick testing of electrochemically active surface area (ECSA), and in hydrogen oxidation reaction (HOR) measurement for comparison of anode catalysts.

The ECSA of the Pt catalyst is calculated from the charge density q_{Pt} (C/cm^{2}electrode) obtained from the CV experiment; the charge required to reduce a monolayer of protons on Pt, Gamma = 210 μC/cm$^2{}_{Pt}$; and the Pt content or loading in the electrode, L in g_{Pt}/cm$^2{}_{electrode}$, (Eq. 14)

$$ECSA\left(\frac{cm^2{}_{Pt}}{g_{Pt}}\right) = \frac{q_{Pt}}{\Gamma . L}$$

Eq. 14

In case of CV, voltamograms were taken from 1 to 0.05 mV, with 100 mV/s. The HOR was made by application of 400, 600, 900, 1225, 1600, and 2025 rpm rotation speed, as shown in **Figure *29*** below. In case of HOR, the potential range was 0-0.3 V and polarization speed was 10 mV/s. Goal of these measurements was to compare the HOR activity of the different $Ti_{0.8}Mo_{0.2}O_2$-C supported anode catalysts to the reference Quintech C-20-PT.

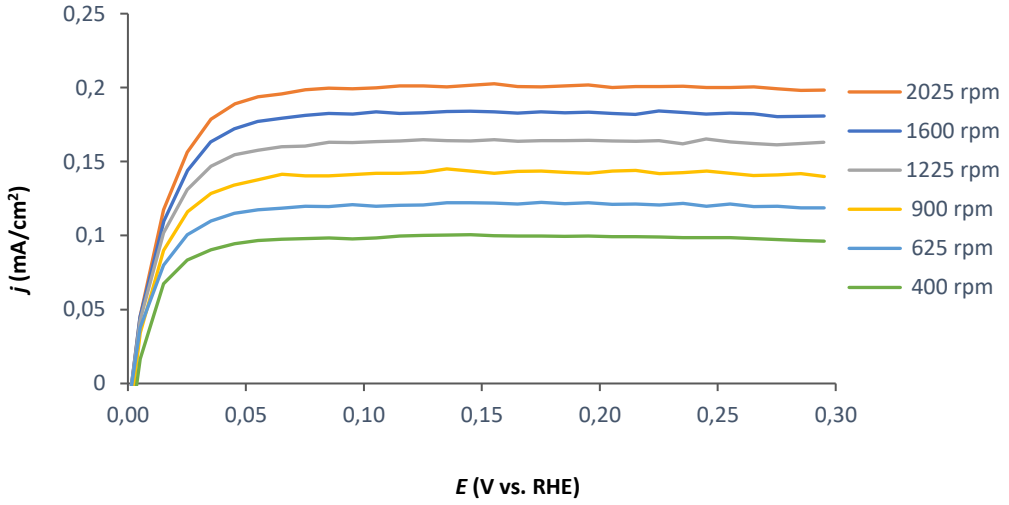

Figure 29. Example of Hydrogen Oxidation Reaction (HOR) analysis for 400, 625, 900, 1225, 1600, and 2025 rpm.

4.3.5. CV measurements on Fuel Cell (FC)

In case of fuel cell, theory of CV measurement was the same as in the 3-electrode system. The most important difference was the lack of a separated reference electrode. Because of it, cable of reference electrode was connected to the cable of working electrode, and they were connected to the BPP of anode with a common inlet. Cathode of the fuel cell was connected as the working electrode. Cables for CV measurements came to the cell from the VMP-300

multichannel potentiostat. That apparatus applied EC-Lab program and potential range was 1-0.05 mV as in case of CVs on RDE. Speed of polarization was 100 mV/s. Slower polarization 10mV/s was possible only on the scaled up 50 cm^2 cell (see later). Gas flow was 200 ml/min H_2 5.0 on anode and 200 ml/min N_2 5.0 on cathode, which were provided by the FCT-150S fuel cell tester.

Those MEAs were measured in CV, which were applied for the Pt loading optimization (DN016-021). Goals of these measurements were to find relation between voltammograms and Pt loading. In case of 50 cm^2 MEA CV was taken with 10mV/s, and from this, ECSA was calculated.

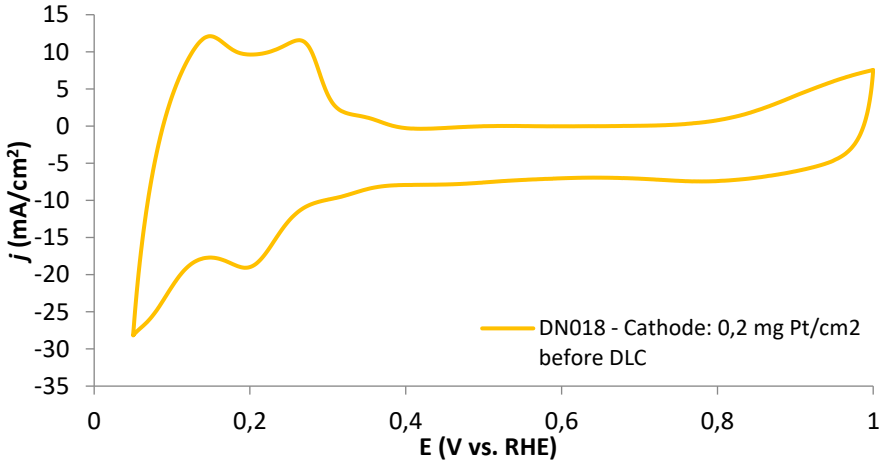

Figure 30. Cyclic voltammetry graph for DN018 at 100 mV/s

4.3.6. Potentiostatic Electrochemical Impedance Spectroscopy (PEIS) measurements on Fuel Cell

Theory of impedance spectroscopy was detailed previously. Goal of these measuremens was to determine the constants of the fitted model circuits (R1+C2/R2) from the (Nyquist plot) impedance spectrums, by application of "Z fit" option of EC-Lab program. The following parameters had to be fixed to carry out a PEIS measurement: i.) cell temperature, ii.) frequency range, iii.) amplitude of alternating voltage (A), iv.) applied fixed voltage (E), v.) gas flows on cathode and on anode, vi.) pressures, vii.) humidifier temperature or gas humidity. The applied measuring conditions are summarized in ***Table 8***:

Table 8. PEIS measuring conditions

Cell temperature:	25 °C
Frequency range:	100 kHz – 10 mHz
A (amplitude):	10 mV
E:	0 V
Cathode gas:	200 ml/min N_2 5.0
Cathode humidifier:	on (25 °C)
Cathode pressure:	atmospheric
Anode gas:	200 ml/min H_2 5.0
Anode humidifier:	on (25 °C)
Anode pressure:	atmospheric

4.3.7. The applied different membrane electrode assembly compositions

The summary of all the MEAs prepared in the project are listed below, in ***Table 9***.

Table 9. Membrane electrode assembly composition for DN001 to DN029

MEA	Cathode catalyst	mg Pt/cm^2	Anode catalyst	mg Pt/cm^2	
DN001	C-20-PT	0.1	C-20-PT	0.1	
DN002	C-20-PT	0.1	C-20-PT	0.1	
DN003	C-20-PT	0.1	C-20-PT	0.1	
DN004	C-20-PT	0.05	C-20-PT	0.05	Preliminary
DN005	C-20-PT	0.05	C-20-PT	0.05	tests
DN006	C-20-PT	0.05	C-20-PT	0.05	
DN007	C-20-PT	0.05	C-20-PT	0.05	
DN008	C-20-PT	0.05	IT025Pt1	0.05	
DN009	C-20-PT	0.05	C-20-PT	0.05	
DN012	C-40-PT	0.1	C-20-PT	0.05	
DN013	C-20-PT	0.05	TiMoOx-75FBP-20PT	0.05	
DN014	C-20-PT	0.05	TiMoOx-75FBP-20PT	0.05	
DN016	C-20-PT	0.05	C-20-PT	0.05	Pt loading
DN017	C-40-PT	0.1	C-40-PT	0.1	optimization

DN018	C-40-PT	0.2	C-40-PT	0.2	
DN019	C-40-PT	0.15	C-40-PT	0.15	
DN021	C-40-PT	0.15	C-20-PT	0.05	
DN022	C-40-PT	0.15	Pt_25TiMoO2-75BP	0.05	Anode
DN023	C-40-PT	0.15	Pt_25TiMoO2-75F*BP	0.05	catalyst
DN024	C-40-PT	0.15	Pt_25TiMoO2-75Vul	0.05	optimization
DN029	C-40-PT	0.15	C-20-PT	0.05	50 cm² MEA

Table shows, that there were four goals of MEA preparation under the project. DN001-014 MEAs were prepared for the preliminary tests, including the practice and configuration of MEA making and the validation of NEDC protocol. After that, next step was the optimization of Pt loading. In this part MEAs contained 0.05, 0.1, 0.2 and 0.15 mgPt/cm^2 both on cathode and on anode side. In case of DN021 different Pt loading between cathode and anode was tested. In anode catalyst optimization part (DN022-24) anode catalyst of the reference MEA (DN021 became the reference – see later) was the variable. Three different carbon – mixed oxide composite supported catalysts were tested (and compared to the reference). Last part of the MEA preparations was the making and testing of 50 cm^2 MEA (the scaling up of DN021).

4.3.8. Scaling up from 16 cm^2 MEA to 50 cm^2 MEA

The project aims to scale up the 16 cm^2 MEA for a more significant dimension to analyze if the MEA keeps a similar performance on a bigger fuel cell. It is important to analyze the fuel cell's performance in a bigger surface area because it is a step closer to using PEM-FC on an industrial scale. The scale up on this project was from 16 cm^2 to 50 cm^2 fuel cell. The MEA preparation followed the same steps for 16 cm^2 (NEDC protocol) using spray coating by AB200 airbrush, and the reference MEA composition was used (Cathode: 0.05 mg Pt/cm^2, Anode: 0.15 mg Pt/ cm^2).

Besides the surface size, another difference between the two fuel cells is a bipolar plate composition. For the 16 cm^2 fuel cell, clean graphite was used as a bipolar plate, while for the 50 cm^2 it was used graphite composite as a bipolar plate. The main difference between the two bipolar places material is that the 16 cm^2 bipolar plates have better conductivity than the 50 cm^2 creating a difference between them.

5. Results and Discussion

5.1.MEA characterization before FC testing

In **Figure *31***, it can be seen the surface of the electrode painted with AB200 airbrush. From this picture, it can be noticed that the platinum (signed by small neongreen points) is homogeneously distributed on the surface of the carbon paper, showing the effectiveness of this method.

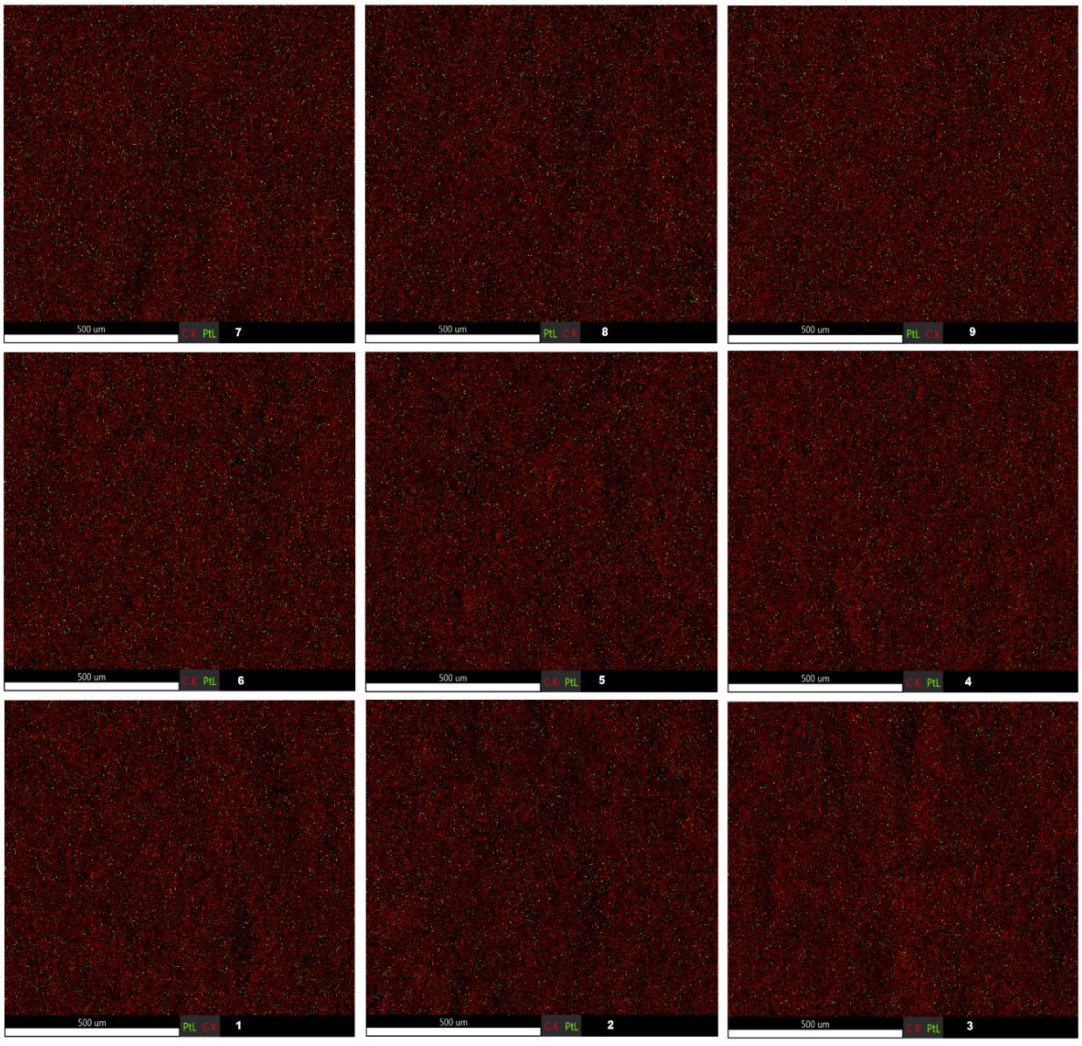

Figure 31. EDS image of the surface of the carbon paper painted with airbrush method.

The Scanning Electron Microscope (SEM) image of the surface of the MEA DN008 is available in **Figure *32*** below. In the image (a), it represents the surface of the MEA, while figure (b) is the figure of the section of the MEA.

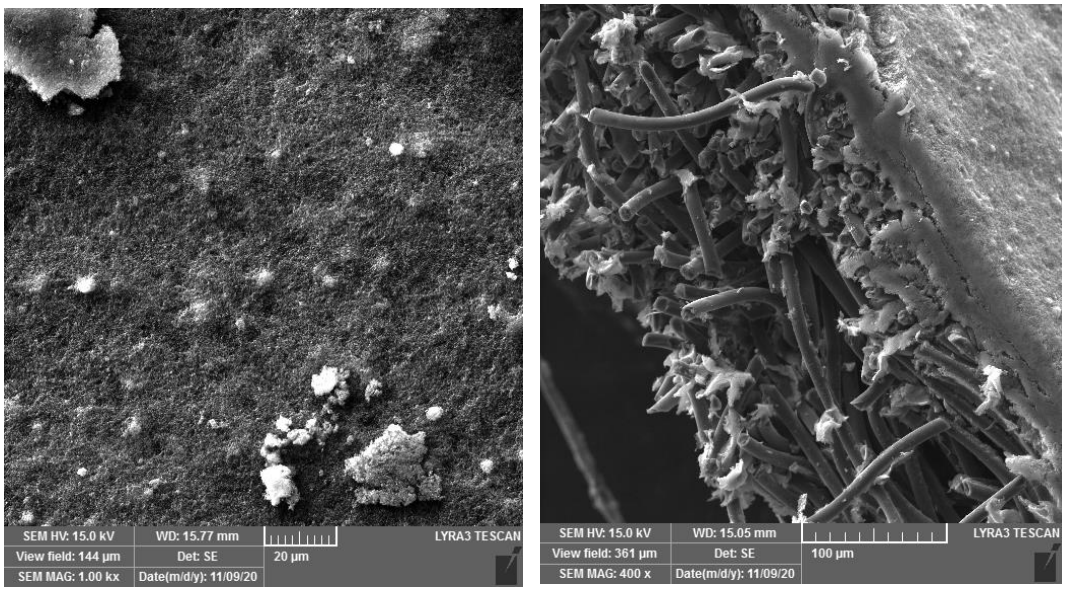

Figure 32. (a) Surface of the DN008 by Scanning Electron Microscope (SEM); (b) Section of the DN008 by Scanning Electron Microscope (SEM)

5.2. Optimization of Pt loading of the MEAs

In order to find the minimal Pt loading for working MEA it was compared five different types of MEA composition (DN016 – Cathode: 0.05 mg Pt/cm^2, Anode: 0.05 mg Pt/ cm^2; DN017 – Cathode: 0.1 mg Pt/cm^2, Anode: 0.1 mg Pt/ cm^2; DN018 - Cathode: 0.2 mg Pt/cm^2, Anode: 0.2 mg Pt/ cm^2; DN019 - Cathode: 0.15 mg Pt/cm^2, Anode: 0.15 mg Pt/ cm^2 and DN021 - Cathode: 0.15 mg Pt/cm^2, Anode: 0.05 mg Pt/ cm^2). From this MEAs it was able to observe the polarization curves on ***Figure 33***.

From this graph we can analyze that for the MEA with composition of DN016 – Cathode: 0.05 mg Pt/cm^2, Anode: 0.05 mg Pt/ cm^2 and DN017 – Cathode: 0.1 mg Pt/cm^2, Anode: 0.1 mg Pt/ cm^2 the results and the average current density (0.589 and 0.874 A/cm^2, respectively) were lower than 1 A/cm^2 and lower compared to the other MEAs. Based on this graph, we can analyze that the other three MEAs have a similar result on the average current density.

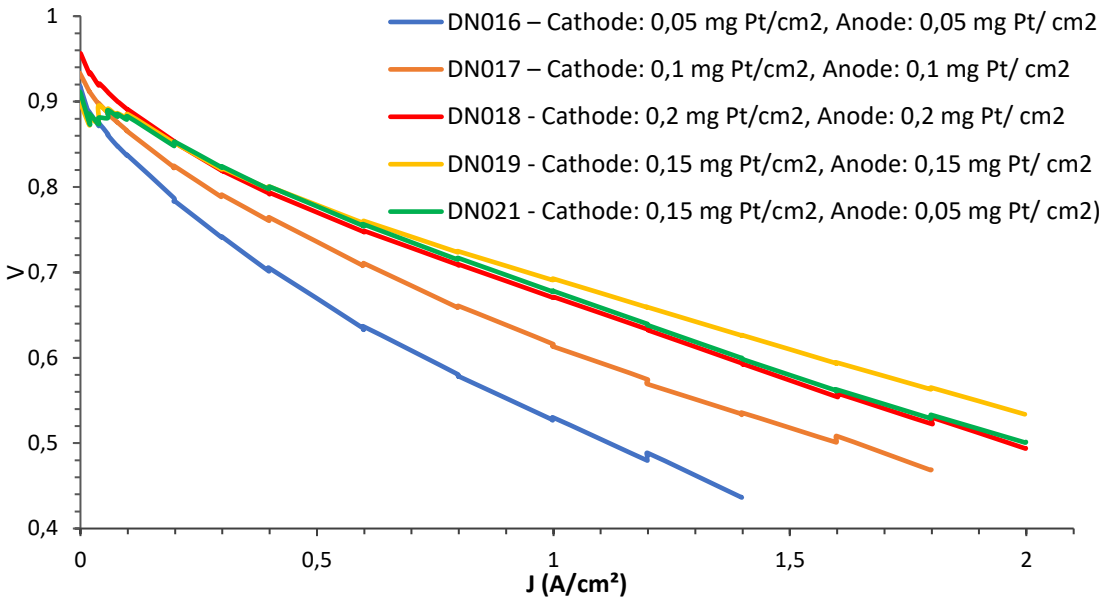

Figure 33. Polarization curves of the descending curves with different Pt loadings for DN016, DN017, DN018, DN019, and DN021.

The five different types of MEA with different Pt loadings selected were analyzed following the NEDC protocol. For this purpose, the polarization curves of the DN016, DN017, DN018, DN019, and DN021 before and after FC-DLC and after regeneration were measured. The polarization curves made it possible to calculate the total degradation rates and reversible and irreversible degradation.

The demonstration of the FC-DLC for the five MEA compositions is presented below. ***Figure 34*** shows the U(V) as dependent on the time for the 1st cycle and 50th cycle and the current density-dependent time for the five different MEA. Based on the results we could see that the current density increases significantly from DN016 to DN021, showing better performances on the DN019 (Cathode: 0.15 mgPt/cm2 C-40-PT; Anode: 0.15 mgPt/cm2 C-40-PT) and DN021 (Cathode: 0.15 mgPt/cm2 C-40-PT; Anode: 0.05 mgPt/cm2 C-20-PT).

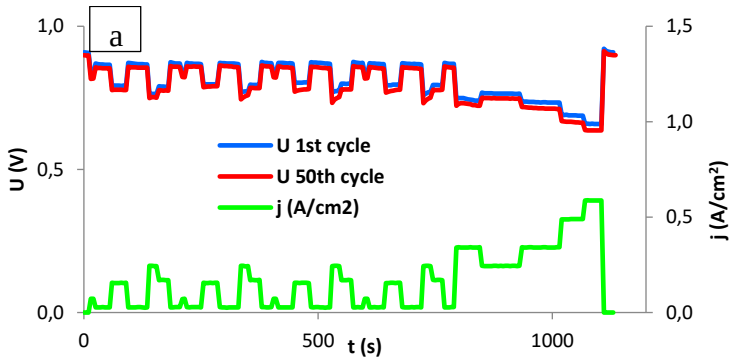

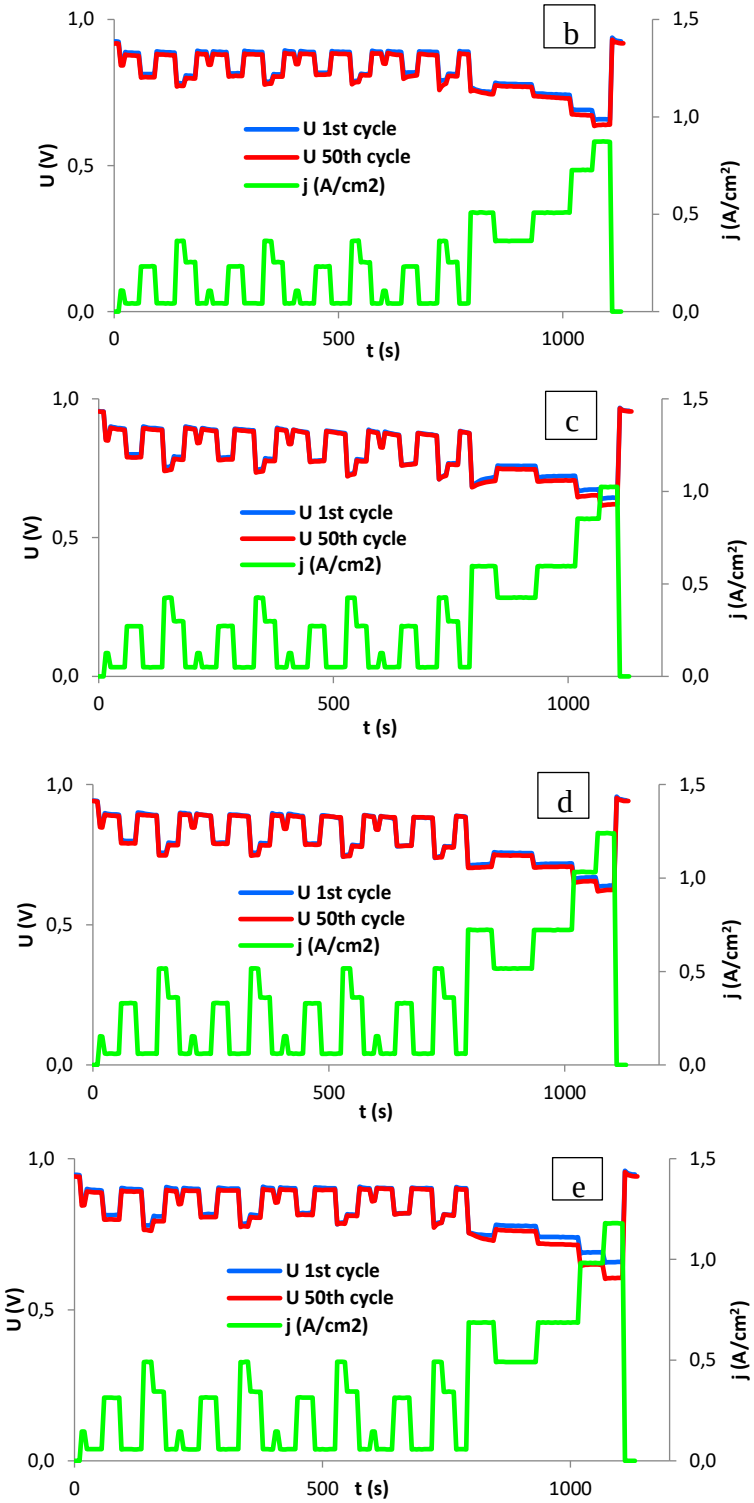

Figure 34. Dynamic Load Cycle Test for the MEA a) DN016, b) DN017, c) DN018, d) DN019, and e) DN021

The determination of power maximum was made to analyze the behavior of the DN016, DN017, DN018, DN019 and DN021 to determine the power maximum achieved for each membrane electrode assembly. The results are shown in ***Figure 35***. We can analyze this graph

that DN019 and DN021 were the MEAs that obtained better performance, achieving 1,1 and 1.107 (W/cm^2) values, respectively.

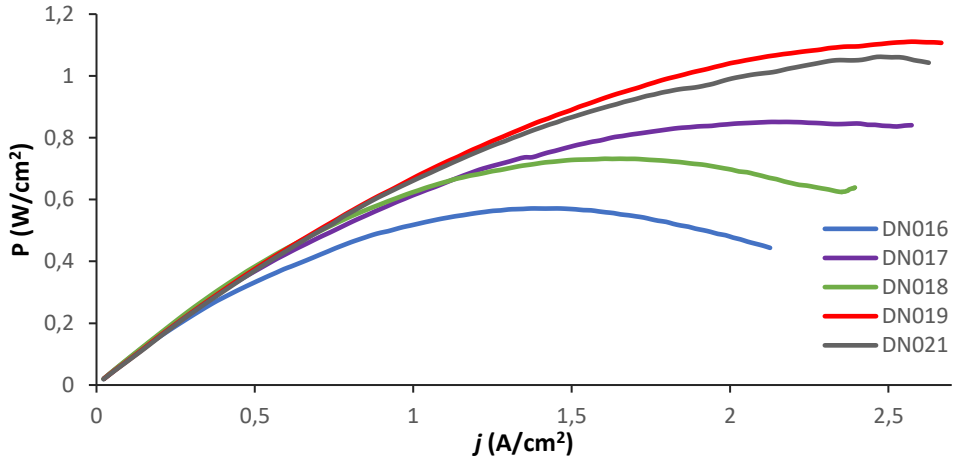

Figure 35. Graph of the behavior of power maximum (W/cm2) for DN016, DN017, DN018, DN019 and DN021

Based on the results from the five different MEA composition, we could analyze that the MEAs which have better performance for power maximum (*W/cm^2*), high value for current density (A/cm^2) at 650mV and degradation rates were the MEAs DN021 and DN019 with the composition of: cathode: 0.15 mgPt/cm^2 C-40-PT; anode: 0.05 mgPt/cm^2 C-20-PT and cathode: 0.15 mgPt/cm^2 C-40-PT; anode: 0.15 mgPt/cm^2 C-40-PT, respectively. We selected the DN021 as our reference MEA because of its less Platinum content and consequently more economic suitability. ***Table 10*** shows a summary of the results for the optimization of Pt loading on the MEAs.

Table 10. Summary of the MEA DN016 to DN021 for degradation rate (µV/h) – total, reversible and irreversible, 100% current density and power maximum.

				100% current density			
MEA	**Total degradation rate (µV/h)**	**Reversible degradation rate (µV/h)**	**Irreversible degradation rate (µV/h)**	**Before DLC**	**After DLC**	**After regeneration**	**Power max**
DN016	1156	0	1156	0.589	0.553	0.491	0.571
DN017	2167	2167	0	0.8745	0.8505	0.809	0.851
DN018	3254	3254	0	1.1810	1.01	0.930	0.731
DN019	1420	337	1082	1.2401	1.125	1.139	1.1
DN021	1909	1909	0	1.135	0.9825	1.144	1.107

Cyclic voltammetry curves were obtained on the DN016 to DN021 electrocatalyst for the cathode made using the FCT-150S apparatus by BioLogic for fuel cell tests integrated with the VMP-300 potentiostat by BioLogic. **Figure *36*** shows the characteristic of the curve for each sample. It can be seen that the electrocatalyst had characteristic hydrogen adsorption/desorption peaks in the potential range between 0 <E < 400 mV except for DN016, which was not possible to observe this behavior. Correspondence was determined between the current density of hydrogen desorption peak, and the Pt loading of cathode.

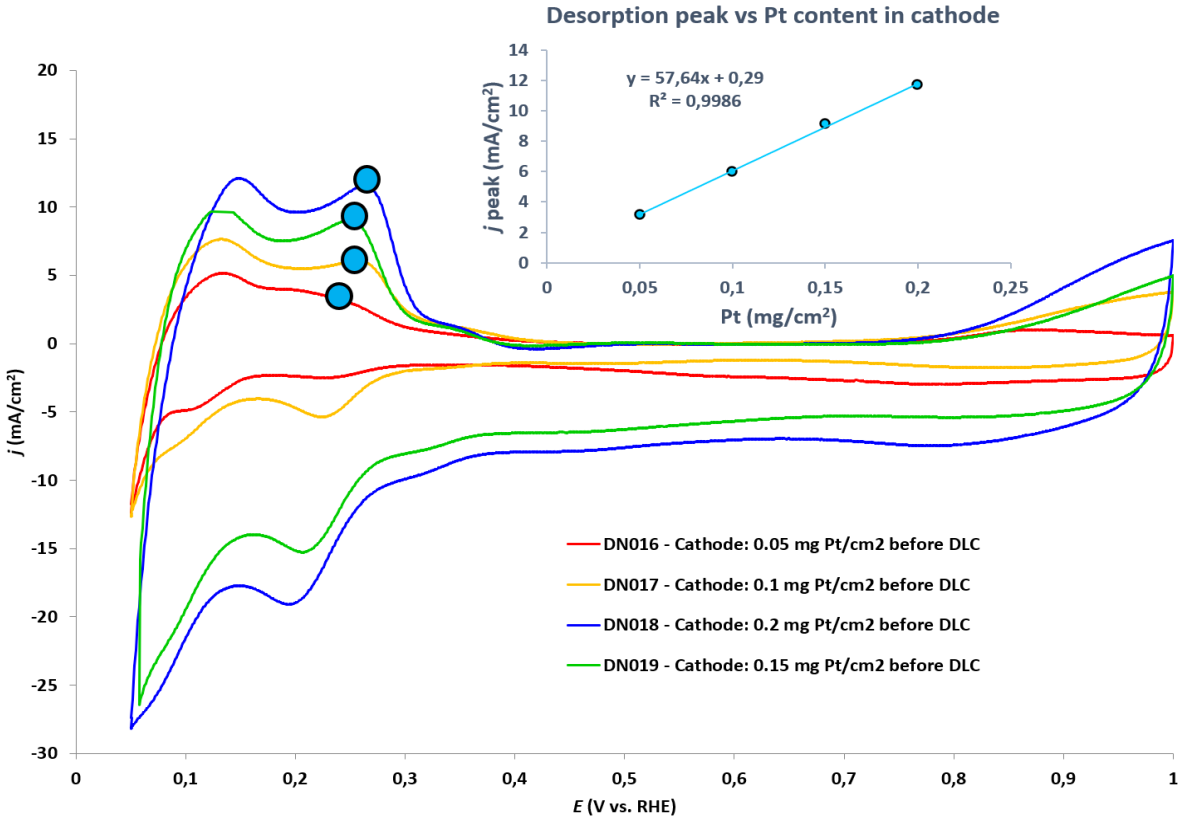

Figure 36. Cyclic voltametric test for DN016, DN017, DN018, DN019, and DN021 before DLC at 100 mV/s

5.3. Fuel Cell testing of anode catalysts

Three different carbon – mixed oxide supported catalysts were tested in fuel cell measurements (DLC test), and the results were compared with our reference MEA, the DN021 (Cathode: 0.15 mgPt/cm^2 C-40-PT; Anode: 0.05 mgPt/cm^2 C-20-PT). The three different MEAs were analyzed on the anode electrode following the 0.05 mgPt/cm^2 loading. The samples were: Pt_25TiMoO2-75BP (DN022), Pt_25TiMoO2-75F*BP (DN023) and Pt_25TiMoO2-75Vul (DN024). ***Figure 37*** shows the four FC-DLC graphs for the MEAs, and ***Figure 38*** shows

the comparison of the polarization curve of the four MEAs. It can be seen on these graphs that the sample which got better results was the Vulcan due to the bigger current density.

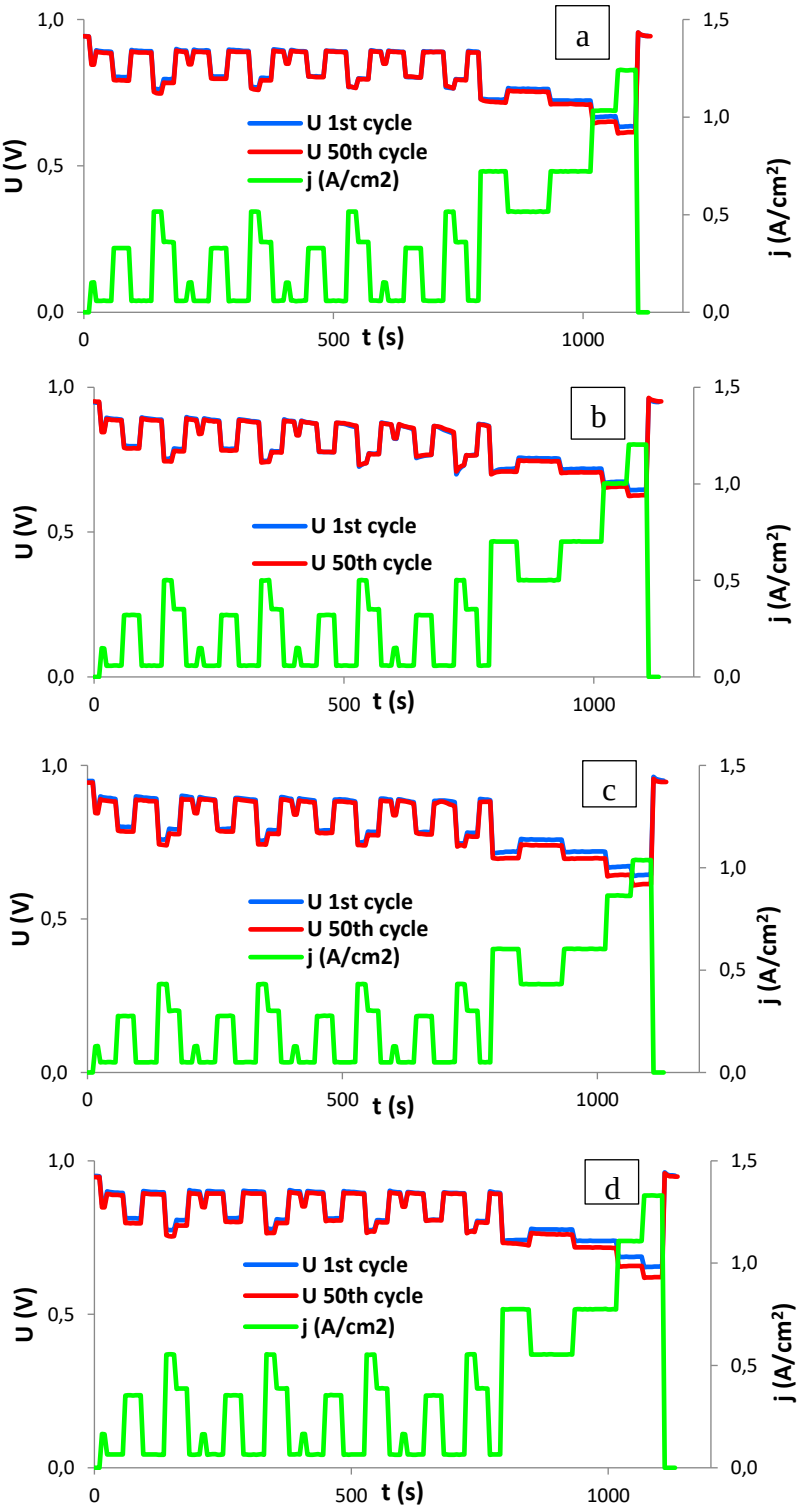

Figure 37. Dynamic Load Cycle test for a) reference MEA (cathode: 0.15 mgPt/cm^2 C-40-PT; anode: 0.05 mgPt/cm^2 C-20-PT) (DN021), b) anode: Pt_25TiMoO2-75BP (DN022), c) anode: Pt_25TiMoO2-75F*FBP (DN023), and d) anode: Pt_25TiMoO2-75Vul (DN024).

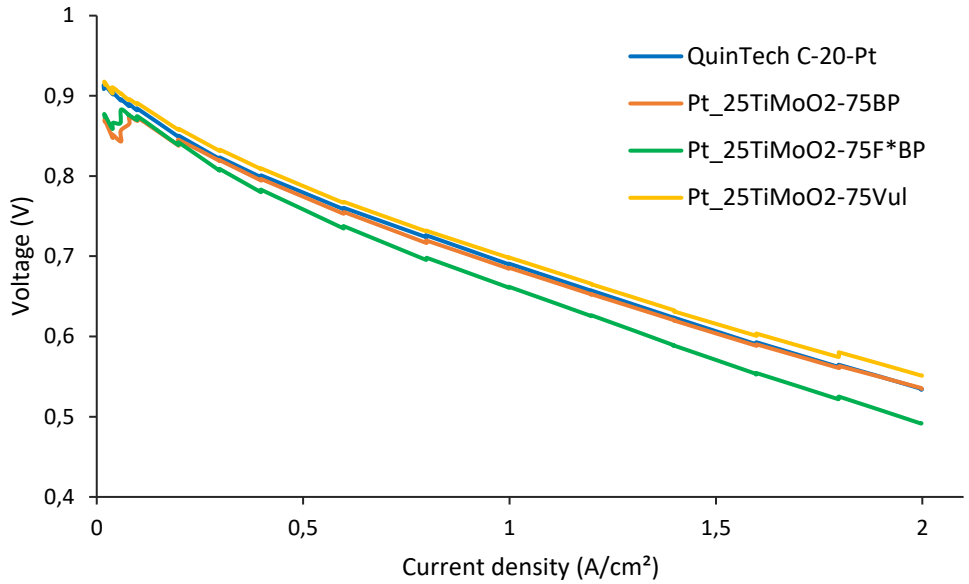

Figure 38. Polarization curve comparison of the reference MEA and Pt_25TiMoO2-75BP, Pt_25TiMoO2-75F*BP, and Pt_25TiMoO2-75Vul.

The results of each current density before and after FC-DLC are listed in ***Table 11*** below. From this value, we can see the Vulcan sample's excellent performance on the current density even after FC-DLC.

Table 11. Values of 100% current density before and after FC-DLC and after regeneration for reference (DN021), Pt_25TiMoO2-75BP(DN022), Pt_25TiMoO2-75F*BP(DN023), and Pt_25TiMoO2-75Vul (DN024) MEAs.

				100% current density			
MEA	**Total degradation rate (μV/h)**	**Reversible degradation rate (μV/h)**	**Irreversible degradation rate (μV/h)**	**Before DLC**	**After DLC**	**After regeneration**	**P_{max}**
DN021	1909	1909	0	1.135	0.9825	1.107	1.107
DN022	556	145	411	1.205	1.088	1.105	1.105
DN023	1327	96	1231	1.039	0.857	0.913	0.913
DN024	2325	1199	1127	1.33	1.315	1.20	1.2

5.4. Hydrogen oxidation reaction of anode catalysts on RDE

HOR test was made to analyze and compare the catalyst ink activity on a rotating disc electrode. The results for the rotating speed of 900 rpm are shown in ***Figure 39***. In case of HOR reference C-20-PT catalyst showed the largest activity and that mixed oxide – C composite

supported sample was the worst, which contained simple BlackPearls 2000 carbon. These results are different to the FC results, in which the DN024 MEA (anode catalyst: Pt_25TiMoO2-75Vul) was the best. On the other hand, HOR results verified that Pt_25TiMoO2-75Vul had the largest activity among the applied mixed oxide – C supported catalysts. Most important lesson of these measurements is that HOR activity is able to make prediction for the catalytic activity, but real efficiency of a catalyst can be shown by the fuel cell measurements and sometimes there can be differences.

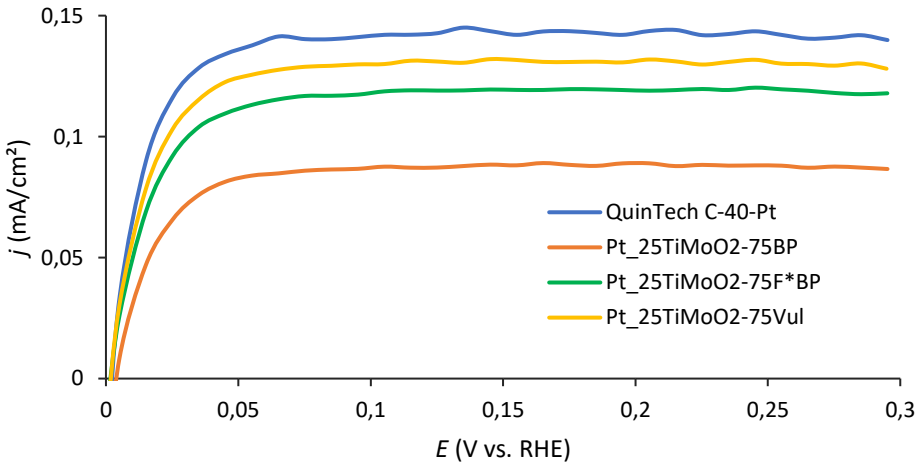

Figure 39. HOR test at 900 rpm for C-20-Pt (reference), Pt_25TiMoO2-75BP, Pt_25TiMoO2-75FBP, and Pt_25TiMoO2-75Vulcan. Speed of the polarization was 10 mV/s

5.5. Potentiostatic Electrochemical Impedance Spectroscopy

The PEIS experiment performs impedance measurements into potentiostatic mode in applying a sinus around a potential E that can be set to a fixed value or relative to the cell equilibrium potential. PEIS experiment for DN017 to DN024 was performed during the project with the goal to evaluate the coefficients for the circuit by following the equivalent circuit (R1+C2/R2) by the application of Zfit analysis. The impedance diagram for DN017 to DN021 before DLC is shown in ***Figure 40*** along the steady-state I x E curve. By this diagram is possible to calculate the components R1, C2, and R2 as using the circuit showed in the ***Figure 41***.

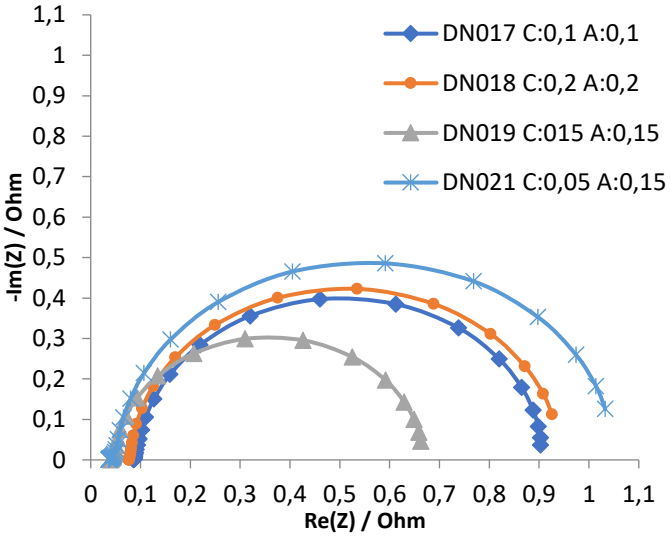

Figure 40. Nyquist plot impedance spectroscopy for DN017 to DN021

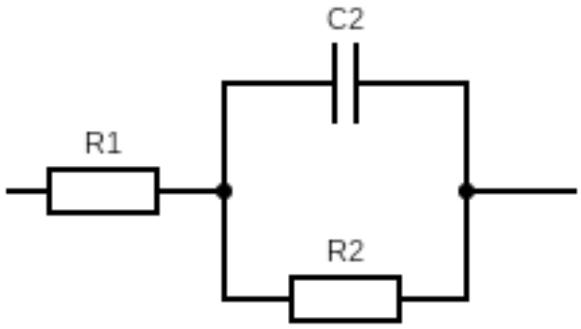

Figure 41. Circuit applied for the calculation of R1, R2 and C2.

In the **Table *12*** and **Table *13***, R1 is the Ohmic Resistance (RΩ), R2 is the polarization resistance Rct and C2 is the double layer capacitance (CdI). If we compare how (RΩ) changes, we can see that the platinum content at the cathode and anode side significantly changes the internal resistance of the cell (the change can be almost double). If R1 is 0.0957 Ohm at 0.1 mg Pt/cm^2, but if the platinum content is increased to 0.15 mg Pt/cm^2, R1 decreases to 0.049 Ohm. This suggests that R1 also includes the resistance of the membrane and the Ohmic resistance of the catalyst layers applied to the cathode and anode side:

$$R\Omega = R_{cathode} + R_{membrane} + R_{anode}$$

For the calculation of the Nafion XL membrane resistance in the 16 cm² cell:

$$R = l / \sigma \times s = 27.5 \text{ x10-4 cm} / 50.5\text{x10-3 Ohm-1cm-1 x 16 cm2} = 0.00340 \text{ Ohm}$$

For DN019, for example, if the resistance of the cathode and the anode part is approx. equal, then a layer of catalyst has a resistance will be the R1 minus 0.0034 Ohm (nafion layer resistance) divided by 2 = 0.0228 Ohms.

Based on the results it can be concluded that the value of RΩ can be reduced (and the efficiency can be increased) if the conductivity of the catalyst layer can be increased. Pt content increases conductivity, but at the same time it increased the price that is the reason why is important to look for additives that can increase the conductivity of the catalyst.

From the results present in **Table *12*** and ***Table 13*** it can be seen that the value of R2 is approximately 10 times greater than R1. Since the total resistance of the cell is the sum of the two resistances:

$$R = R\Omega + Rct$$

Therefore, is easier to increase the efficiency of the cell by reducing the Rct than for reducing R1. The increasing of C is generally proportional to the increase in effective surface area, but may also vary with chemical composition. **Table *12*** and ***Table 13***, we can see that C increases in proportion to the amount of Pt in the cathode. The PEIS experiment was performed to the anode mixed oxide experiment as well, and the results for the components R1, C2, and R2 are available in the **Table *12*** below.

Table 12. PEIS coefficients (R1, C2, R2) for DN017 to DN021 before and after FC-DLC

PEIS coefficients	**R1 (Ohm)**	**C2 (F)**	**R2 (Ohm)**	**Resistance cathode**	**Resistance anode**
DN017 – before DLC	0.0957	0.914	0.806	0.04615	0.04615
DN017 – after DLC	0.093	0.776	1.019	0.0448	0.0448
DN018 - before DLC	0.081	2.401	0.852	0.0388	0.0388
DN018 - after DLC	0.107	1.942	1.043	0.0518	0.0518
DN019 - before DLC	0.049	1.891	0.612	0.0228	0.0228
DN019 - after DLC	0.0377	1.554	16.25	0.0171	0.0171
DN021 - before DLC	0.05376	2.015	0.968	0.0228	0.0276

DN021 - after DLC	0.0505	0.272	0.77	0.0228	0.0243

Table 13. PEIS coefficients for reference (DN021), Pt_25TiMoO2-75BP (DN022), Pt_25TiMoO2-75F*BP (DN023) and Pt_25TiMoO2-75Vul (DN024) before and after FC-DLC

PEIS coefficients	**R1 (Ohm)**	**C2 (F)**	**R2 (Ohm)**	**Resistance cathode**	**Resistance anode**
DN021 - before DLC	0.0537	2.015	0.968	0.0228	0.0276
DN021 - after DLC	0.0505	0.272	0.77	0.0228	0.106
DN022 - before DLC	0.1318	0.1202	0.683	0.0228	1.104
DN022 - after DLC	1.13	1.77	1.922	0.0228	0.043
DN023 - before DLC	0.0693	0.1995	1.132	0.0228	0.013
DN023 - after DLC	0.0394	0.3959	25.21	0.0228	0.092
DN024 - before DLC	0.1185	2.298	0.85	0.0228	0.122
DN024 - after DLC	0.1482	1.022	27.68	0.0228	0.0276

Since the EIS measurements are made at a potential of U = 0 and an alternating potential 10 mV, the cathode initially has a very small amount of hydrogen. If a CV is plotted under these conditions, the concentration of H_2 increases with polarization. Hydrogen adsorption and desorption on the platinum surface is a reversible process and EIS measurements are made around this point. At the anode, there will be protons from the hydrogen gas, which will move towards the cathode through the membrane and be reduced to hydrogen gas and leave the cell when mixed with nitrogen.

For determination of R1 there are more possible ways. It was introduced above, that one of these solutions is to fit curve to the impedance spectrum by the EC-Lab program. On the other hand, R1 can be calculated from the slope of the linear part of the polarization curves. Importance of that method is the following:

R1 and R2 depend on the temperature. PEIS measurements were carried out at 25°C, but it would be necessary to know the R1 values on the reaction temperature. From slopes of the linear part of polarization curves, ohmic resistance can be obtained, and R1 results can be compared at 25 and at 80°C in case of all MEAs. The **Figure *42*** shows how the R1 from the polarization curve was calculated. **Table *14*** introduces the results:

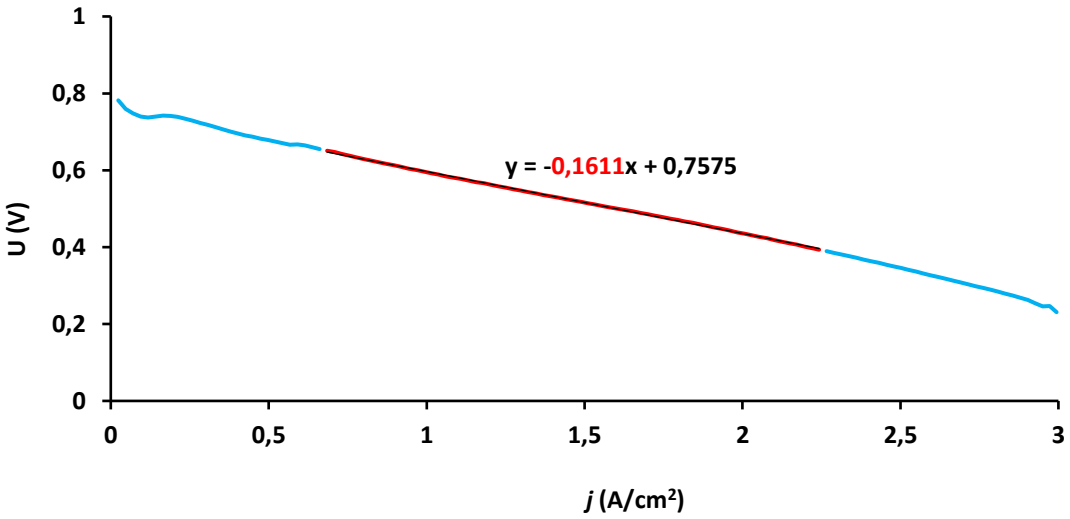

Figure 42. Demonstration of the calculation of R1 from the slope of the linear part of polarization curve.

Table 14. R1 coefficients of MEAs at 25°C (from PEIS) and at 80°C (from polarization curves)

PEIS coefficients	R1 (Ohm) from PEIS 25ºC	R1 (Ohm) from polarization 80ºC
DN017 – before DLC	0.0957	0.2010
DN017 – after DLC	0.093	0.2284
DN018 - before DLC	0.081	0.1844
DN018 - after DLC	0.107	0.2343
DN019 - before DLC	0.049	0.1617
DN019 - after DLC	0.0377	0.1684
DN021 - before DLC	0.05376	0.1860
DN021 - after DLC	0.0505	0.2009
DN022 - before DLC	0.1318	0.1580
DN022 – after DLC	1.13	0.1684
DN023 – before DLC	0.0693	0.1765
DN023 – after DLC	0.0394	0.1684
DN024 – before DLC	0.1185	0.1570
DN024 – after DLC	0.1482	0.1716

For simplification of the analysis, the following table (**Table *15***) contains only the "before" values:

Table 15. Comparison of R1 coefficients of MEAs at 25 and 80°C and the influence of mixed oxide composite anode support

MEA	R1 25°C (Ohm)	R1 80°C (Ohm)	mgPt/cm^2	Anode catalyst
DN017 – before DLC	0.0957	0201	0.1	C-40-Pt
DN018 - before DLC	0.081	0.1844	0.2	C-40-Pt
DN019 - before DLC	0.049	0.1617	0.15	C-40-Pt
DN021 - before DLC	0.05376	0.186	0.05	C-20-PT
DN022 - before DLC	0.1318	0.158	0.05	Pt_25TiMoO2-75BP
DN023 – before DLC	0.06703	0.1765	0.05	Pt_25TiMoO2-75F*BP
DN024 – before DLC	0.06347	**0.157**	0.05	Pt_25TiMoO2-75Vul

In most MEAs, R1 increased by the rising of temperature. Higher ohmic resistance was calculated on those MEAs, which contained only commercial QuinTech C-20-PT or C-40-PT on anode. In that case there was correlation between R1 values, obtained at 25 and at 80 °C, which is visualized on **Figure *43***. Lowest R1 resistance on 80°C was calculated in case of DN024 MEA, which was the best sample under the whole project.

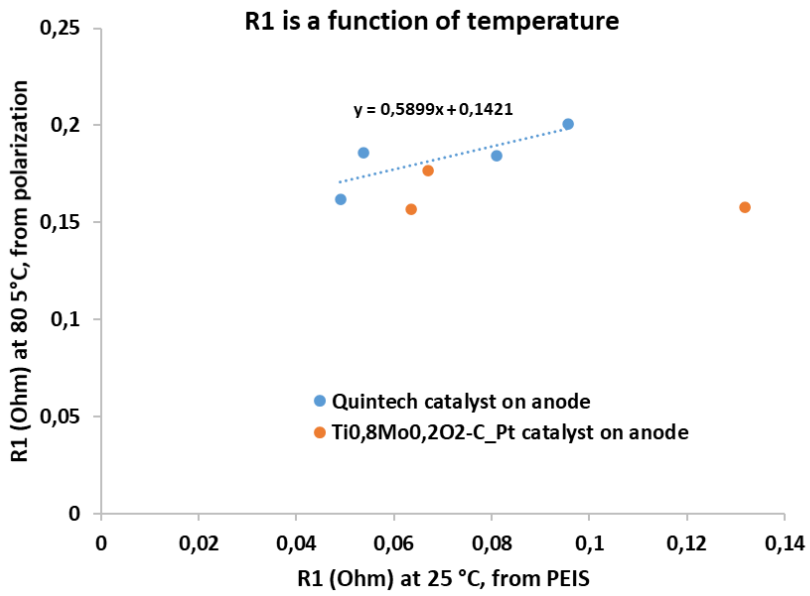

Figure 43. Correlation between R1 at 25 and at 80°C

Good properties of this MEA can be explained:

- MEA contained only 0.05mgPt/cm^2 on anode and 0.15mgPt/cm^2 on cathode.
- Mixed oxide – carbon anode catalyst support had a semiconductor effect, which hindered the increment of R1 on the reaction temperature, in the MEA.
- Vulcan carbon was used for the preparation of catalyst support. That type of carbon has the best conductivity among the applied carbons.

5.6. Scaling up from 16 cm^2 to 50 cm^2

The reference MEA (DN021) was scaled up from 16 cm² MEA to 50 cm² MEA to analyze if the fuel cell keeps the same performance in a bigger cell as in a small cell. The representation draws of the 50 cm² MEA is shown in ***Figure 44***. The experiment on 50cm² MEA was made using the reference composition and denoted as DN029, and the results was compared with DN021. The experiment followed the NEDC protocol by activation of the MEA, polarization before DLC, DLC test, polarization after DLC, regeneration, polarization after regeneration and determination of power maximum.

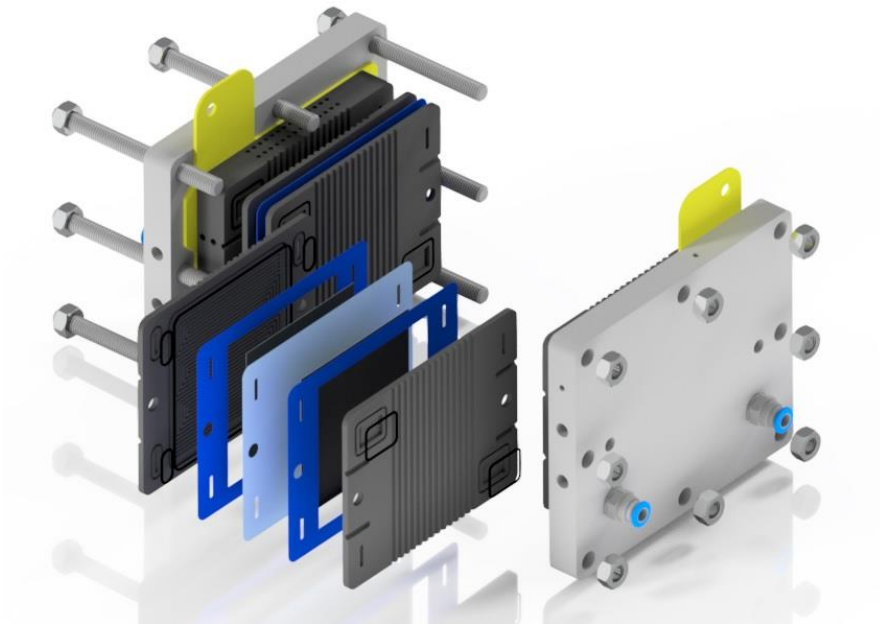

Figure 44. 50cm² PEM fuel cell (stack version) 3D model

The results of the polarization curve are shown in the ***Figure 45***. It is noted that the average current density at 650 mV was inferior than in the smaller cell. The average current density for 16 cm² and 50 cm² before FC-DLC at 650 mV was 1,135 A/cm² and 0.5095 A/cm², respectively.

The average current density for 16 cm² and 50 cm² after FC-DLC at 650 mV was 0.9825 A/cm² and 0.3795 A/cm², respectively. The reason of this different result can be the different material applied on the bipolar plates which affects the overall conductivity of the PEM fuel cell.

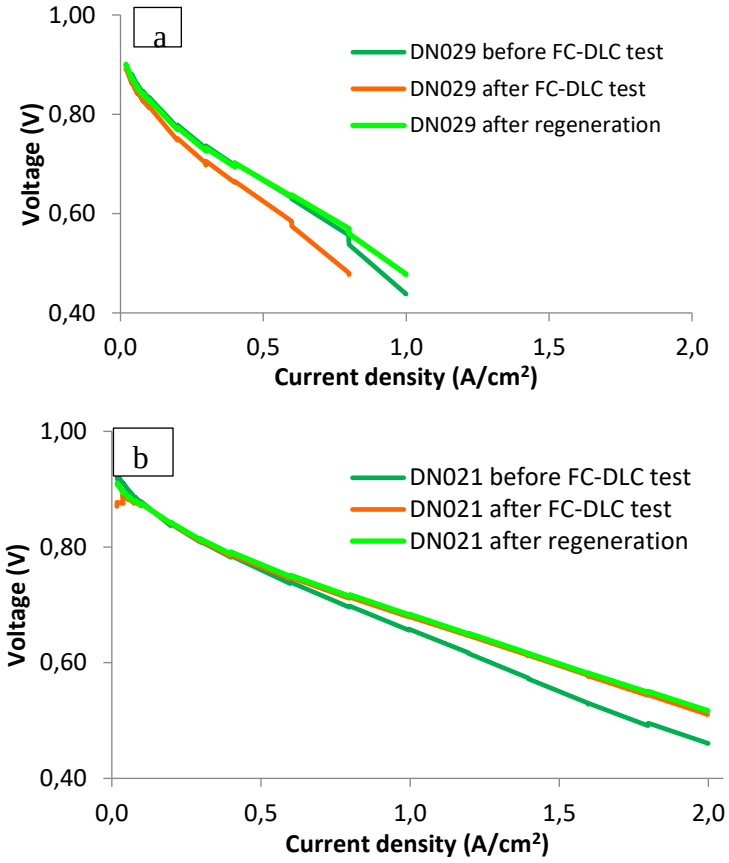

Figure 45. a) Polarization curves before and after DLC and after regeneration for DN029. b) Polarization curves before and after DLC and after regeneration for DN021

The power maximum was measured in the 50 cm² fuel cell and the comparison result with the 16cm² is shown in the ***Figure 46*** below. The power maximum for DN029 was inferior than for the DN021 it could be for the lower conductivity of the bigger bipolar plate.

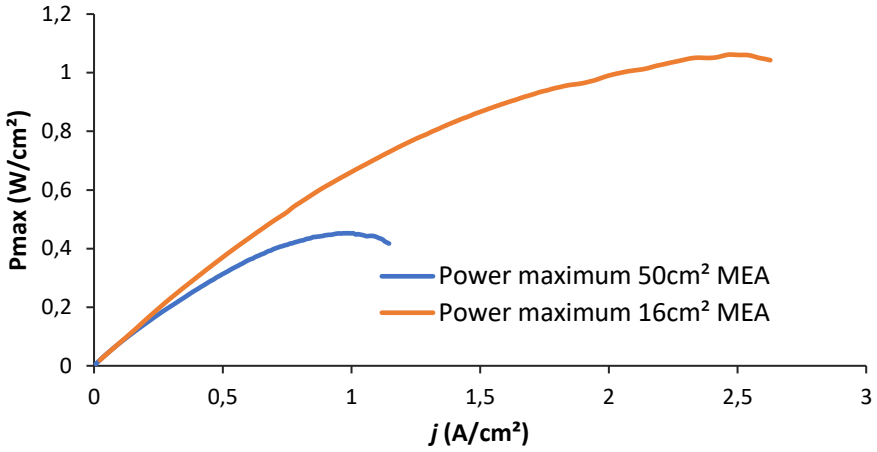

Figure 46. Determination of power maximum for 16cm² and 50cm² MEA

Electrochemistry tests were done to analyze the performance of the fuel cell. For that, ***Figure 47*** shows the CV at 100mV before and after DLC for the16 cm² and 50 cm² MEA. The results for both MEA were similar, showing that the composition of the bipolar plate does not have a strong influence on the CV.

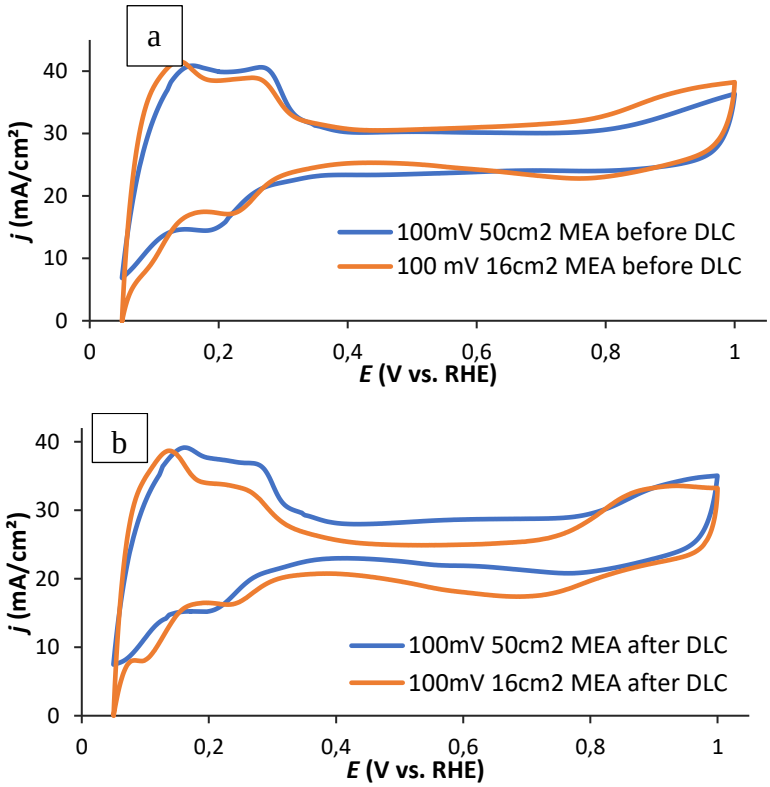

Figure 47. 100 mV/s CV for 16 cm² and 50 cm² MEA before and after DLC test

Figure *48* shows the CV for 10 mV/s for 50 cm² and 16 cm² MEA. It is possible to see, however, that for 10mV/s there is a difference on the CV for each MEA size. CV of the 16 cm²

MEA is too flat for evaluation, but well understandable H_2 adsorption and desorption peaks were obtained on the voltamogram of 50 cm^2 MEA in case of 10 mV/s scanning speed.

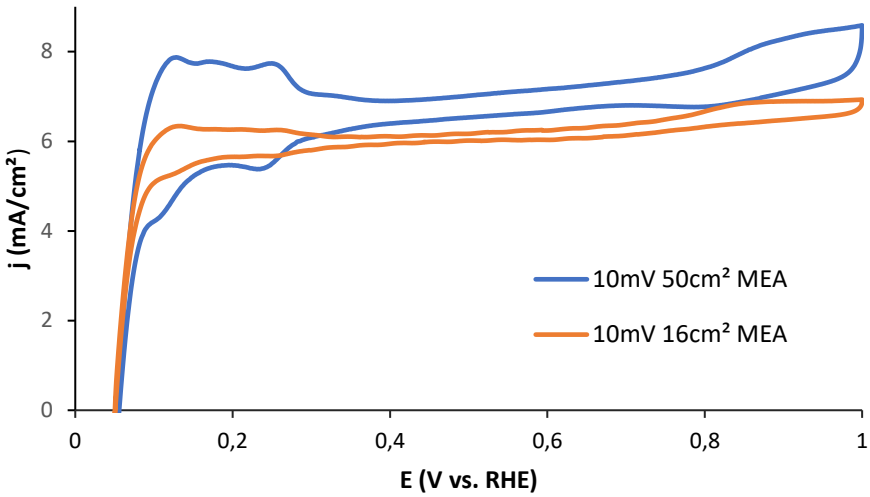

Figure 48 - 10mV/s CV for 16 cm² and 50 cm² after DLC

In case of 10mV/s CV of 50cm^2 MEA value of ECSA was calculated. In this case currents were 3 ranges higher, but in the end, obtained result was in the good range and it was comparable to usual ECSAs which are measured on 3 electrode cell. The calculation was according to ***Table 16***.

Table 16. Calculation of electrochemical active surface area

H_2 desorption peak integral:	1631.48 mC
t_1:	171.19 s
t_2:	200.96 s
Baseline:	25.4917 mA
Baseline integral:	(200.96 s – 171.19 s)*20.4917 mA = 758.96 mC
Difference of integrals:	1631.48 mC – 758.96 mC = 872.5156 mC = 872515.6 mC
Charge of H+ adsorption	210 mC/cm^2
Surface	872515.6 mC / 210 mC/cm^2 = 4154.84 cm^2 = 0.415484 m^2
Pt loading of cathode:	0.15 mg/cm^2 = 0.00015 g/cm^2

A_{GDE}:	50 cm^2
Pt content of GDE:	50 cm^2 * 0.00015 g/cm^2 = 0.0075 g
ECSA:	0.415484 m^2 / 0.0075 g = **55.40 m^2/gPt**

The obtained result is less than the usually required 60-80 m^2/gPt, but it can be explained the large resistance of the cell. On the other hand, scaling up increased the double layer capacity. Equation 15 shows that current (I) of cyclic voltammetry is the product of double layer capacitance (Cdl) and the scanning speed (v).

$$I = Cdl * v \qquad \textbf{Eq. 15}$$

Because of this, the capacitance increased, but scanning speed was able to be decreased from 100mV/s to 10mV/s. That is the explanation, that why 10mV/s CV of 50 cm^2 MEA could be evaluated.

6. Summary

PEM fuel cells are able to produce current with good efficiency, at low temperature. They are not containing moving parts, and they have zero emission, because the only byproduct is the water. The primary aim of my thesis work was to establish the methodology of testing of fuel cell electrocatalysts under realistic working conditions in a fuel cell test equipment. Optimization of the manufacturing of GDEs, development of measuring protocol, reduction of the noble metal content of MEAs, addition of Pt to different catalyst supports and their fuel cell testing, and scaling up of the cell were among the goals of my work.

First step was the development of the manufacturing of MEAs. I used the so-called spray coating method in which catalyst ink was painted by airbrush (AB200) onto the surface of gas diffusion layers (GDLs). I managed to develop a well applicable protocol. Even catalyst distribution on GDEs was verified by SEM images.

New European Driving Cycle (NEDC) is an EU harmonized measuring protocol, which was developed for the PEMFC MEA testing of fuel cell vehicles. Beyond taking of polarization curves, the method gives exact description about the stability tests, regeneration and calculation of the degradation of MEAs, and about the analysis of the effect of working parameters. By implementing the whole protocol in our measuring system it became possible to compare the MEAs made by me in this project, according to an international standard method.
Pt loading was 0.5 mg/cm^2 both on cathode and on anode side on those MEAs, which were applied for testing and configuration of NEDC protocol. Next phase of the work was the optimization of the Pt content of MEA. Commercial catalysts (QuinTech C-20-PT and C-40-PT) were applied for this. The goal was to reach 1 A/cm2 current density on 650mV voltage (NEDC protocol applies that voltage for calculation), and to reduce Pt content bellow 0.35g/kW (Pt content of commercial PEM fuel cells). Final, reference MEA was the DN021, which contained 0,15mgPt/cm^2 on cathode and 0,05mgPt/cm^2 on anode. Its power-proportional Pt loading was 0.27gPt/kW.

In the next step of experimental work the novel $Ti_{0,8}Mo_{0,2}O_2$-C composite supported Pt electrocatalysts developed int he host research group were characterized by fuel cell testing. Pt loading of MEAs was 0.15 mg/cm^2 on cathode and 0.05 mg/cm^2 on anode, as a result of previous optimization. The composite supported electrocatalysts, which provide good tolerance against CO poisoning and promise enhanced long-term stability, were used on the anode side, while commercial C-40-PT was applied on the cathode. During comparison of composite

supports made by application of different types of active carbon a Vulcan type carbon containing sample turned out to be the best performer. The MEA containing 25TiMoO2-75Vul and reached 1.33A/cm^2 current density on 650mV with a power-proportional Pt loading of 0.23gPt/kW.

Connection of the fuel cell tester with multichannel potentiostat resulted in an unique measuring station, in which cyclic voltammetry (CV) and Potentiostatic Electrochemical Impedance Spectroscopy (PEIS) measurement of MEAs can be realized. In case of CV measurements on a fuel cell, resistance of the whole system has to be taken into account, which is negligible in 3 electrode electrochemical cells. Because of that, only those CV results could be used, where speed of cyclization was higher (100mV/s). It is interesting, that scaling up compensated the effect of resistance; taking of voltammogram was possible in the 50cm^2 cell on 10mV/s and the results were suitable for evaluation.

Parameters of appropriately selected model circuits were derived from the PEIS data. Results showed, that those MEAs were the bests (DN019 and DN021), in which ohmic resistance (R1) was the least (approximately 0.05 ohm). From the obtained data, catalyst layer resistances were calculated in case of all MEAs, both on anode and on cathode side. Ohmic resistance on working temperature was determined from the slope of polarization curves. Comparison of R1 values on 25 and on 80°C revealed, that advanageous properties of the best DN024 MEA are obtained by the simultaneous effect of the following factors: i.) the small Pt loading, ii.) semiconductor properties of mixed oxide – composite support and iii) presence of good conducting Vulcan type carbon in the composite support.

In scaling up I made and tested 50cm^2 size MEA instead of previous 16cm^2 sized ones. Pt loading was the same as in the reference DN021 (C:0.15mgPt/cm^2, A:0.05mgPt/cm^2). BPPs in 50cm^2 cell were made of grafhite-polymer composite, whose conductivity was only the 20% of the conductivity of pure graphite. Because of this reason, surface proportional power of the larger cell was much worse, than in case of 16cm^2 cell. Bipolar plates need to be made of graphite for further measurements. Experiments showed, that capacitance of the cell increased by the scaling up. Because of this reason, voltamogram with 10mV/s was able to be taken in the 50 cm^2 cell, and result could be evaluated (ECSA calculation).

There are more opportunities in application of impedance spectroscopy; development of protocols is in progress. Next step of the scaling up is among the further plans; this will be the exact configuration of the measuring method of fuel cell stack.

7. Összefoglalás

A PEM tüzelőanyag-cellák alacsony hőmérsékleten, jó hatásfokkal képesek elektromos áramot termelni. Mozgó alkatrészt nem tartalmaznak és nincs káros anyag kibocsátásuk, mivel az egyetlen keletkező melléktermék a víz. Diplomamunkám során több, a témához kapcsolódó kérdést vizsgáltam. A kitűzött célok között szerepelt a gázdiffúziós elektródok előállításának optimalizálása, a mérési protokoll kialakítása, a membránelektród-együttesek nemesfém-tartalmának csökkentése, különféle katalizátor hordozók platinázása és tüzelőanyag-cellás vizsgálata, valamint a cella méretnövelése.

A legelső lépés membránelektród-együttesek előállításának a kidolgozása volt. Az úgynevezett spray coating technikát alkalmaztam, amelyben a katalizátor tintát festékszóró pisztollyal (AB200) vittem fel a gázdiffúziós rétegek felületére. Sikerült kialakítanom egy jól alkalmazható protokollt. A kész elektródok egyenletes katalizátor eloszlását a SEM felvételek visszaigazolták.

A New European Driving Cycle (NEDC) egy EU által harmonizált mérési protokoll, amit tüzelőanyag-cellás járművekhez használt PEMFC MEA-k vizsgálatához fejlesztettek ki. A módszer a polarizációs görbék felvételén túl pontos leírást ad a MEA-k stabilitásvizsgálatáról, regenerálásáról, a degradáció számításáról, valamint a működési paraméterek hatásának vizsgálatáról is. Mindezt sikerült átültetni a saját rendszerünkre.

A NEDC protokoll kialakításához olyan MEA-kat készítettem, amelyek a katódon és az anódon is 0,5 mg/cm^2 platinát tartalmaztak. A munka következő fázisa a MEA Pt tartalmának optimalizálása volt. Kereskedelmi forgalomban kapható katalizátorokat (QuinTech C-20-PT és C-40-PT) használtam. A cél az 1 A/cm^2 áramsűrűség elérése volt 650mV feszültségen (a NEDC protokoll ezt a feszültséget veszi alapul), valamint a 0,35 g/kW alatti Pt tartalom (a kereskedelmi forgalomban kapható PEM cellák Pt tartalma). A végső, referencia MEA a DN021 lett, amelynek borítottsága a katódon 0,15mgPt/cm^2, az anódon pedig 0,5 mgPt/cm^2. A MEA teljesítményarányos Pt tartalma 0,27g/kW.

A kísérleti munka következő lépése a saját katalizátorok előállítása, vizsgálata és tüzelőanyag-cellás tesztelése volt. A MEAk Pt borítottsága a korábbi optimalizálás eredményeként a katódon 0,15 mg/cm^2, az anódon 0,05 mg/cm^2 volt. $Ti_{0,8}Mo_{0,2}O_2$-C kompozit hordozós katalizátorokat vizsgáltam anód oldalon (a katódra C-40-PT katalizátort tettem). A kompozitok többféle aktív szén felhasználásával készültek. A legjobb katalizátorhordozónak a Vulcan típusú szenet tartalmazó minta bizonyult. Az ebből készült MEA (DN024) Pt tartalma 0,23g/kW volt, 650mV-on 1,33A/cm^2 áramsűrűséggel. A katalizátorok elkészítéséhez a

hordozókra 20 m/m% Pt vittem fel $NaBH_4$ redukciós módszerrel. Az elkészült katalizátorokat a tüzelőanyag-cellás tesztek előtt háromelektródos elektrokémiai cellában vizsgáltam, ahol CV, illetve HOR méréseket végeztem.

A tüzelőanyag cella teszter berendezés összekapcsolása a többcsatornás potenciosztáttal egy olyan egyedi mérőállomás kialakítását tette lehetővé, amelyben sikerült kiviteleznem a MEA-k CV mérését, illetve a potenciosztatikus elektrokémiai impedancia spektroszkópiás (PEIS) mérését. A tüzelőanyag-cellában a teljes rendszer ellenállása számottevő a háromelektródos rendszerrel öszehasonlítva, ahol mindez elhanyagolható. Ez volt az oka, hogy a MEAkról csak a 100mV/s sebességgel felvett voltammogramokat lehetett kiértékelni. A Pt tartalom optimalizálásához használt MEAk esetén sikerült kimérni, hogy a hidrogén deszorpciós csúcs áramsűrűsége hogyan aránylik a katód Pt borítottságához.

A PEIS mérésekkel sikerült a különböző MEA-k esetén a cellában lejátszódó folyamatokra illeszthető modell áramkörök paramétereit meghatározni. Az eredmények azt mutatták, hogy azok a MEA-k voltak a legjobbak (DN019, DN021 és DN024), ahol az ohmikus ellenállás (R1) a legalacsonyabb volt (0,065 ohm alatt). A kapott adatokból minden mért MEA esetén kiszámítottam a katalizátor réteg ellenállását anód és katód oldalon is. Az ohmikus ellenállást üzemi hőmérsékleten a polarizációs görbék lineáris szakaszának meredekségéből határoztam meg. A 25 és 80°C hőmérsékleten kapott R1 értékeke összehasonlítása megerősíti a feltételezést, hogy a legjobbnak bizonyult DN024 MEA kedvező tulajdonságait a következő tényezők együttes hatása okozhatja: i.) a kis Pt tartalom, ii.) a vegyes-oxid kompozit hordozó félvezető tulajdonsága és iii.) a kompozit hordozóban található, jó vezetőképességű Vulcan típusú szén jelenléte

A méretnövelés során korábbi 16 cm^2-es MEA-k helyett 50cm^2-es MEA-t állítottam elő, illetve teszteltem. A MEA összetétele a referencia DN021-nek megfelelő volt (K:0,15mgPt/cm^2, A:0,05mgPt/cm^2). A nagy cellában a bipoláris lemezek anyaga grafit-polimer kompozit volt, amelynek a vezetőképessége kb. 20%-a a kisebb cellában használt tiszta grafit BPP-nek. Ennek megfelelően a nagy cella felületarányos teljesítménye messze elmaradt a 16 cm^2-es celláétól. A későbbiekben a bipoláris lemezeknek grafitból kell készülnie. A kísérletek megmutatták továbbá, hogy CV mérés esetén a MEA méretnövelésével a cella kapacitása is nőtt, ezért itt 10 mV/s sebességgel is értékelhető voltamogramot tudtam felvenni, amelyből elektrokémiailag aktív felületet határoztam meg.

Az impedancia spektroszkópia alkalmazása a további kutatások szempontjából számos lehetőséget kínál; a pontos protokollok kialakítása jelenleg is folyamatban van. A további tervek között szerepel a cellaköteges tesztek mérési módszerének a pontos kidolgozása.

8. Acknowledgment

Many thanks to my supervisor, Dr. András Tompos, director of the Institute of Materials and Environmental Chemistry. He provided the opportunity to making my theses in the Renewable Energy Research Group and his experience was useful help in my work.

I also wish to express my thanks to Dr. Imre Miklós Szilágyi for helping my work as internal consultant.

I am also grateful to my external consultant, Dr. Gábor Pál Szijjártó for direct controlling and helping my work and teaching me the necessary preparative processes, FC testing and electrochemical measurements.

My thanks are due to all members of the Renewable Energy Research Group. Their experience, knowledge and patience were also useful to complete my theses. I wish to express my thanks to Dr. Zoltán Pászti and Dr. Irina Borbáth for lecturing of my dissertation and to our technician, Ildikó Turi for helping in preparations.

I want to say thanks to Dana Radu and Andrei Kuncser (National Institute of Material Phisics – Romania), and Dr. Mihaela Florea (University of Bucharest, Faculty of Chemistry) for the SEM and TEM measurements.

I also want to express my thanks to Dr. András Suplicz (Technical University, Department of Polymer Technology), and to Zoltán Boros (H-ION Kft.) for manufacturing of the 50 cm^2 cell.

The financial supports by the following projects are greatly acknowledged:

VEKOP-2.3.2-16-2017-00013. “The excellence of strategic R & D workshops, Material science excellence workshop: development of environmentally friendly processes for efficient use of renewable energy and raw materials and for controlled release of their energy content”.

Project no. NNE130004 has been implemented with the support provided from the National Research, Development and Innovation Fund of Hungary, financed under the TR-NN-17 funding scheme.

Project no. 2017-2.3.7-TÉT-IN-2017-00049 has been implemented with the support provided from the National Research, Development, and Innovation Fund of Hungary, financed under the TÉT-IN-2017 funding scheme.

This work was performed within the framework of the “Holistic design of fuel cell electrocatalysts for the least power applications” (CATALEAST) M-ERA.NET project. Project No. NNE 131270 has been implemented with the support provided from the National Research, Development and Innovation Fund of Hungary financed under the M-ERA.NET funding scheme.

References

[1] M. A. S. B Viswanathan, Fuel Cells, principles and applications, Chennai: CRC Press LLC, Taylor and Francis Group, 2007.

[2] B. Rath and J. Marder, "Powering the future - power from sunlight: photovoltage.," *Advanced Materials & Processes,* vol. 165, no. 5, pp. 28-29, 2007.

[3] W. Vielstich, A. Lamm and H. Gasteiger , Handbook of Fuel Cells: Fundamentals, Technology, Applications, 2003.

[4] Y. Eren, O. Erdinc, M. Uzunoglu and B. Vural, "A fuzzy logic based supervisory controller for an FC/UC hybrid vehicular power system," *International Journal of Hydrogen Energy,* vol. 34, no. 20, pp. 8681-8694, 2009.

[5] P. Breeze, Power Generation Technologies, Newnes, 2014.

[6] "Fuel Cell Electric Buses," [Online]. Available: https://www.fuelcellbuses.eu/wiki/fuel-cells-hydrogen-and-fuel-cells/4-components-pem-fuel-cell.

[7] H. Ebrahimian, S. Barmayoon, M. Mohammadi and N. Ghadimi, "The price prediction for the energy market based on a new method," *Ekonomska Istrayivanja / Economic Research,* vol. 31, no. 1, 2018.

[8] A. Maher, "A simple mathematical model of perfomance for proton exchange membrane fuel cells," *International Journal of Sustainable Energy,* vol. 26, no. 3, pp. 79-90, 2007.

[9] C. Gittleman, F. Coms and Y. Lai, "Membrane Durability: Physical and Chemical Degradation," in *Polymer Electrolyte Fuel Cell Degradation* , New York, 2012, pp. 15-88.

[10] S. Peighambardoust, S. Rowshanzamir and M. Amjadi, "Review of the proton exchange membranes for fuelcell applications," *International Journal of Hydrogen Energy,* pp. 9349-9384, 2010.

[11] A. J. Appleby and F. R. Foulkes, Fuel cell handbook, New York: Van Nostrand Reinhold, 1989.

[12] A. Baroutaji, M. Sajjia, A. G. Olabi and J. G. Carton, "Materials in PEM Fuel Cells," in *Reference Module in Materials Science and Materials Engineering*, 2015.

[13] H. De-Chin, Y. Pei-Jung, L. Feng-Jiin, H. Shu-Ling, H. Kan-Lin, C. Yen-Cho, W. Chun-Hsing, C. Wen-Chen and T. Fang-Hei, "Effect of Dispersion Solvent in Catalyst Ink on Proton Exchange Membrane Fuel Cell Perfomance," *International Journal of Electrochemical Science,* vol. 6, pp. 2551-2565, 2011.

[14] M. Perry, R. Darling, S. Khandoi, T. Patterson and C. Reiser, "Operating Requirements for Durable Polymer-Electrolyte Fuel Cell Stacks," in *Polymer Electrolyte Fuel Cell Durability*, New York, 2009, pp. 399-417.

[15] T. Ralph, "Catalysis for Low Temperature Fuel Cells," *Platinum Metals Rev.,* vol. 46, no. 3, p. 117, 2002.

[16] K. Hyun, C. M. Kyung, K. Jeong, J. H. Yeon, L. J. Kyung, K. Y. Na, N. W. Suk, L. Dong-Hee, C. EunAe, L. Kwan-Young and K. Y. Jin, "Highly efficient and durable TiN nanofiber electrocatalyst supports," *Nanoscale,* vol. 7, no. 44, 2015.

[17] B. Bladergroen, H. Su, S. Pasupathi and V. Linkov, "Overview of Membrane Electrode Assembly Preparation Methods for Solid Polymer Electrolyte Electrolyzer," 2012.

[18] V. Mathur and J. Crawford, "Fundamentals of Gas Diffusion Layers in PEM Fuel Cells," in *Fuel Cell Science and Technology*, New Dehli, India, pp. 116-128.

[19] D. Brett and N. Brandon, "Bipolar plates: the lungs of the PEM fuel cell," *The fuell cell review*, pp. 15-23, February/March 2005.

[20] Y. Zhao, Y. Mao, W. Zhang, Y. Tang and P. Wang, "Reviews on the effects of contaminations and research methodologies for PEMFC," *International Journal of Hydrogen Energy*, vol. 45, no. 43, pp. 23174-23200, 2020.

[21] S. K. Kamarudim, F. Achmad and W. R. Daud, "Overview on the application of direct methanol fuel cell (DMFC) for portable electronic devices," *International Journal of Hydrogen Energy*, vol. 34, no. 16, pp. 6902-6916, 2009.

[22] L. Guoliang, T. Wen-Chin and W. Sheng, "Sulfonated silica coated polyvinylidene fluoride electrospun nanofiber-based composite membranes for direct methanol fuel cells," *Materials & Design*, vol. 193, p. 108806, 2020.

[23] Z. Xuxin, Y. Wenxiang, W. Qixing, S. Hongyuan, L. Zhongkuan and F. Huide, "High-temperature passive direct methanol fuel cells operating with concentrated fuels," *Journal of Power Sources*, vol. 273, pp. 517-521, 2015.

[24] C. Wang, "Principles of Direct Methanol Fuel Cells for Portable and Micro Power," in *Mini-Micro Fuel Cells*, 2008, pp. 235-242.

[25] F. Samimi and M. Rahimpour, "Direct Methaanol Fuel Cell," in *Methanol Science and Engineering*, Shiraz, 2018, pp. 381-397.

[26] Y. Tsukagoshi, H. Ishitobi and N. Nakagawa, "Improved performance of direct methanol fuel cells with the porous catalys layer using highly-active nanofiber catalyst," *Carbon Resources Conversion*, vol. 1, no. 1, pp. 61-72, 2018.

[27] M. Hosseinpour, M. Sahoo, M. Perez-Page, S. R. Baylis, F. Patel and S. M. Holmes, "Improving the performance of direct methanol fuel cells by implementing multilayer membranes blended with cellulose nanocrystals," *International Journal of Hydrogen Energy*, vol. 44, no. 57, pp. 30409-30419, 2019.

[28] E. Gülzow, "Alkaline fuel cells: a critical view," *Journal of Power Sources*, vol. 61, no. 1, pp. 99-104, 1996.

[29] L. Chia-Lien, C. Cheng-Ping, G. Yi-Hsuan, Y. Tsung-Kuang, S. Yu-Chuan, W. Pen-Cheng, H. Kan-Lin and T. Fan-Gang, "High-performance and low-leakage phosphoric acid fuel cell with synergic composite membrane stacking of micro glass microfiber and nano PTFE," *Renewable Energy*, vol. 134, pp. 982-988, 2019.

[30] S. Ganguly, S. Das, K. Kargupta and D. Banerjee, "Optimization of performance of PAFC stack using reduced order model with integrated space marching and electrolyte inferencing," *Computer Aided Chemical Engineering* , vol. 31, pp. 1010-1014, 2012.

[31] I. Dincer and M. A. Rosen, "Exergy Analysis of Fuel Cell Systems," in *EXERGY*, 2007, pp. 303-324.

[32] D. Eapen, S. Suseendiran and R. Rengaswamy, "Phosphoric acid fuel cells," in *Compendium of Hydrogen Energy*, Chennai, 2016, pp. 57-70.

[33] W. Jung-Ho, "Applications of proton exchange membrane fuel cell systems," *Renewable and Sustainable Energy Reviews,* vol. 11, no. 8, pp. 1720-1738, 2007.

[34] B. Wu, M. A. Parkes, V. Yufi, L. Benedetti , S. Veismann , C. Wirsching, F. Vesper, R. F. Martinez-Botas , A. J. Marquis, G. J. Offer and N. P. .. Brandon, "Design and testing of a 9.5 kWe proton exchange membrane fuel cellesupercapacitor passive hybrid system," *international journal of hydrogen energy,* vol. 39, pp. 7885 - 7896, 2014.

[35] W. Reaves and M. A. Hoberecht, "Proton Exchange Membrane (PEM) Fuel Cell Status and Remaining Challenges for Manned Space-Flight Applications".

[36] K. He, C. Zhang, Q. He and L. Jackson, "Effectiveness of PEMFC historical state and operating mode in PEMFC prognosis," *International Journal of Hydrogen Energy,* vol. 45, no. 56, pp. 32355-32366, 2020.

[37] B. James and A. Spisak, in *Mass Production Cost Estimation of Direct H2 PEM Fuel Cell Systems for Transportation Applications: 2012 Update*, Strateg. Anal. Inc., 2014, pp. 1-62..

[38] L. P. L. Carrette, K. A. Friedrich, M. Huber and U. Stimming, "Improvement of CO tolerance of proton exchange membrane (PEM) fuel cells by a pulsing technique," no. 3, pp. 320-324, 2 November 2001.

[39] Y. Devrim, A. Albostan and H. Devrim, "Experimental investigation of CO tolerance in high temperature PEM fuel cells," *International Journal of Hydrogen Energy,* no. 43, pp. 18672-18681, 2018.

[40] G. Gergely, "Irányított felületi reakciók alkalmazása tüzelőanyag-cellák elektrokatalizátorainak fejlesztéséhez," in *Msc dissertation,* Budapest, 2016, pp. 16-18.

[41] S. Mohammed Rezaei Niya and M. Hoorfar, "Study of proton exchange membrane fuel cells using electrochemical impedance spectroscopy technique - A review," *Journal of Power Sources,* vol. 240, pp. 281-293, 2013.

[42] J. Wu, X. Z. Yuan, H. Wang, M. Blanco, J. J. Martin and J. Zhang, "Diagnostic tools in PEM fuel cell research: Part I Electrochemical techniques," *International Journal of Hydrogen Energy,* vol. 33, pp. 1735-1746, 2008.

[43] I. Pivac, B. Simic and F. Barbir, "Experimental diagnostics and modeling of inductive phenomena atlow frequencies in impedance spectra of proton exchange membranefuel cells," *Journal of Power Sources,* vol. 365, pp. 240-248, 2017.

[44] S. Pasupathi, J. C. C. Gomez, H. Su, H. Reddy, P. Bujlo and C. Sita, "HT-PEMFC Modeling and Design," in *Recent Advances in High-Temperature PEM Fuel Cells*, 2016, pp. 32-54.

[45] L. Sun, R. Ran, G. Wang and Z. Shao, "Fabrication and perfomance test of a catalyst-coated membrane from direct spray deposition," *Solid State Ionics,* vol. 179, pp. 960-965, 2008.

[46] A. El-kharouf, T. J. Mason, D. J. L. Brett and B. G. Pollet, "Ex-situ characterisation of gas diffusion layers for proton exchange membrane fuel cells," *Journal of Power Sources,* vol. 218, pp. 393-404, 2012.

[47] X. Liang, G. Pan, L. Xu and J. Wang, "A modied decal method for preparing the membrane electrode assembly of proton echange membrane fuel cells," *Fuel,* vol. 139, pp. 393-400, 2015.

[48] S. Shin, J. -K. Lee, H. -Y. Ha, S.-A. Hong, H. -S. Chun and I. -H. Oh, "Effect of the catalytic ink preparation method on the performance of polymer electrolyte membrane fuel cells," *Journal of Power Sources,* vol. 106, pp. 146-152, 2002.

[49] M. Roser, "Our World in Date," [Online]. Available: https://ourworldindata.org/cheap-renewables-growth#:~:text=With%20each%20doubling%20of%20the%20installed%20cumulative%20capacity%20the%20price,A%20decline%20of%2099.6%25..

[50] M. S. Yazici, S. Dursun, I. Borbath and A. Tompos, "Reformate gas composition and pressure effect on CO tolerant Pt/Ti0.8Mo0.2O2eC electrocatalyst for PEM fuel cells," *International Journal of Hydrogen Energy,* 2020.

[51] "IRENA (Internnational Renewable Energy Agency)," [Online]. Available: https://www.irena.org/newsroom/articles/2020/Jun/How-Falling-Costs-Make-Renewables-a-Cost-effective-Investment.

Appendix

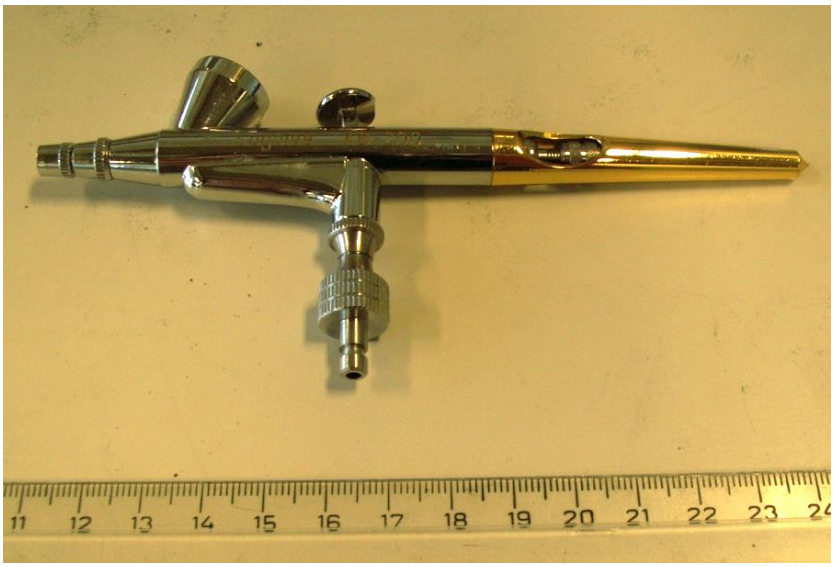

Figure 49. AB200 airbrush from Conrad Electronic SE applied for the paint on the carbon paper.

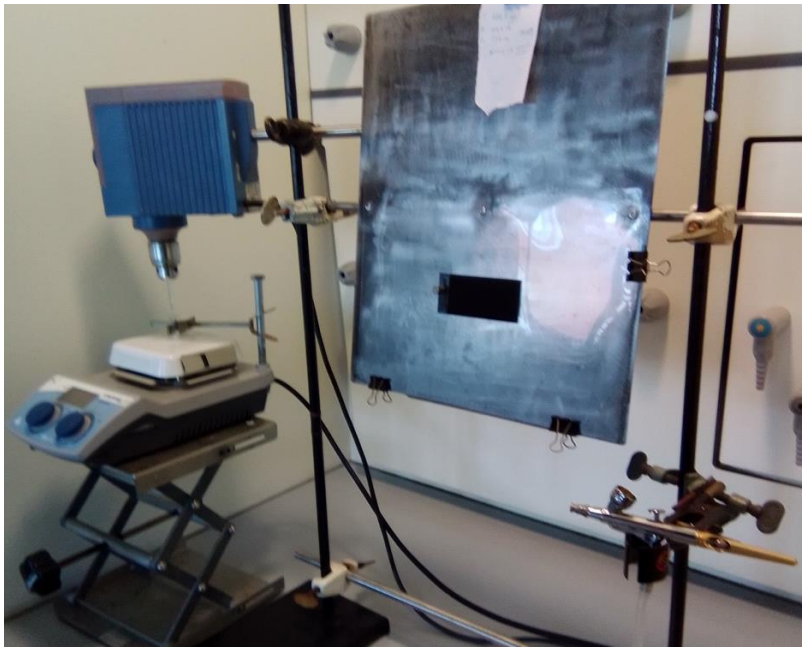

Figure 50. Workplace of the application of the catalyst ink over the carbon paper applying AB200 airbrush.

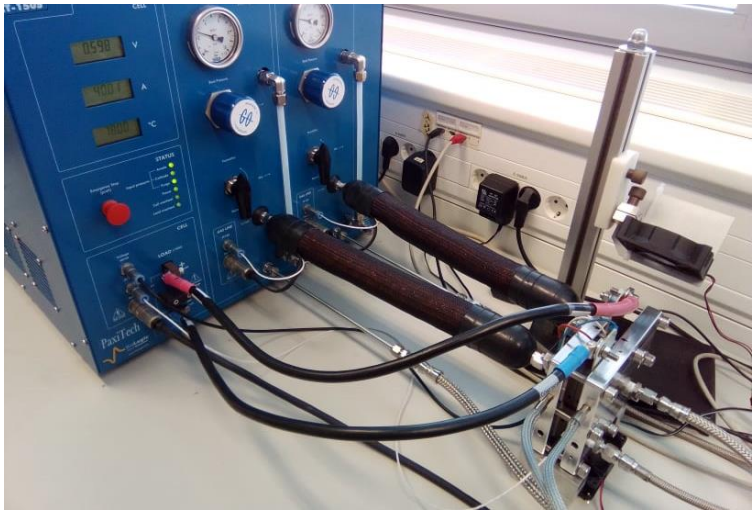

Figure 51. FCT-150S apparatus by BioLogic applied for the fuel cell measurements.

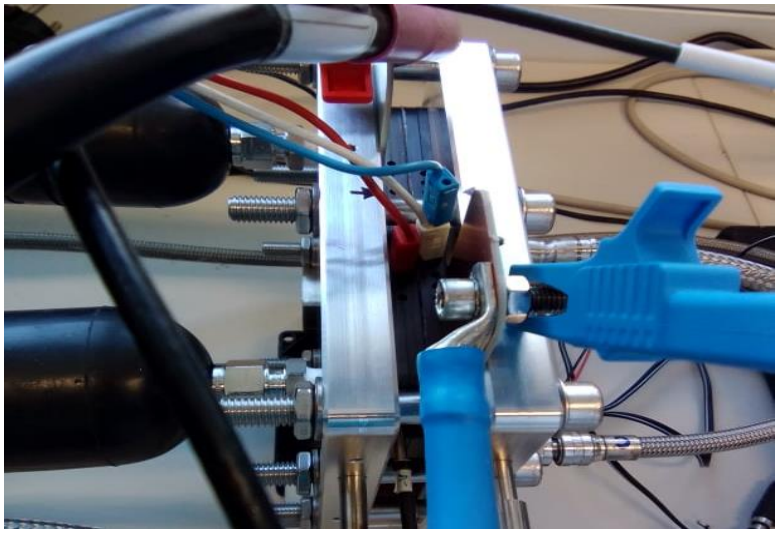

Figure 52. Close image of the connections of the fuel cell.

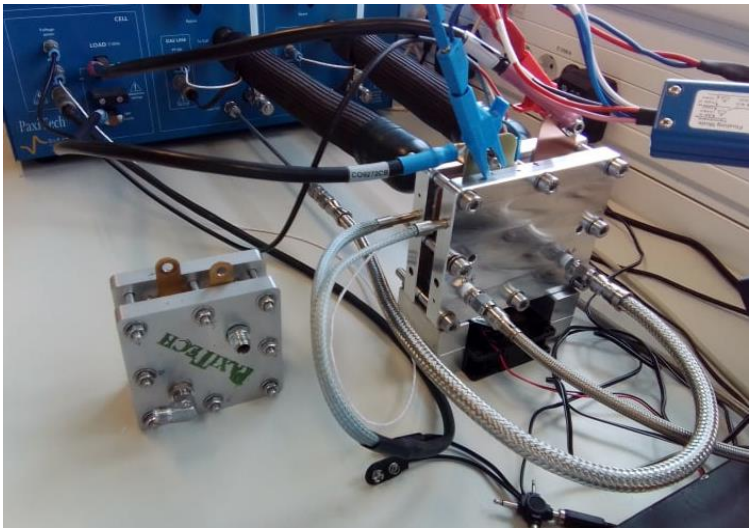

Figure 53. Comparison of the 16 cm² (left) and 50 cm² (right) fuel cell.

Figure 54. Fuel cell stack of the 50 cm² fuel cell

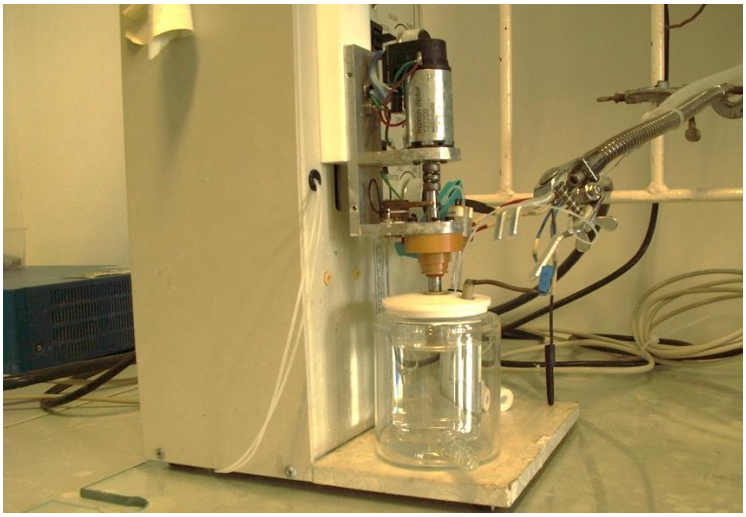

Figure 55. RRDE-3A Rotating disc electrode was applied for HOR measurements

Table 17. Chemicals used in platinum loading

Material	Chemical formula/ Abbreviation	Purity	Manufacturer/Distributor
Hexachloroplatinic acid hexahydrate	$H_2PtCl_6*6H_2O$	35,5%	Sigma-Aldrich
Ethanol	C_2H_5OH	99,95%	Molar Chemicals
Sodium borohydride	$NaBH_4$	99,99	Molar Chemicals
Ethylene glycol	$(CH_2OH)_2$	99,8%	Molar Chemicals
Hydrochloric acid (37%)	HCl	-	Molar Chemicals

Table 18. Gases used in electrochemical measurements

Gas	Chemical formula/ Abbreviation	Purity	Manufacturer/Distributor
Argon	Ar	5,0	Linde Gas Hungary Co
Hydrogen	H_2	5,0	Linde Gas Hungary Co
Carbon monoxide	CO	4,7	Messer Hungarogas

Table 19. Chemicals and materials used in electrochemical measurements

Material	Chemical formula/ Abbreviation	Purity	Manufacturer/ Distributor
Milli-Q Water	H2O	Millipore, 18.2 MΩ cm	TTK AKI
Sulphuric acid (96%)	H2SO4	PA	Merck
2-propanol	i-C3H5OH	99.9%	Molar Chemicals
5% Nafion dispersion	-	-	Dupont
10 μm aluminium-oxide powder	Al_2O_3	99.99%	Nanografi
20 wt.% Pt-based Catalyst	20 wt.% Pt/C	-	Quintech
40 wt.% Pt-based Catalyst	20 wt.% Pt/C	-	Quintech

Table 20. Chemicals and materials used for PEMFC

Part	Parameter	Type	Manufacturer
FC tester	150 A $I_{max.}$, 5V $U_{max.}$	FCT-150S	BioLogic
Cell	16 cm^2, 3 Nm bolt torque	SC G Series	PaxiTech
Carbon paper	40x40x0.250 mm	H23C6	Freudenberg
Catalyst	20 m/m% Pt	C-20-PT	QuinTech
Polymer for cat. ink	5 m/m% Nafion® content	NS05	QuinTech